J. Synchrotron Rad. (1997). **4**, 316–333

Atomic and Molecular Physics Using Synchrotron Radiation – the Early Years

K. Codling

J. J. Thomson Physical Laboratory, University of Reading, Reading RG6 6AF, UK. E-mail: k.codling@reading.ac.uk

(Received 21 July 1997; accepted 29 August 1997)

The field of atomic and molecular photoionization has undoubtedly been transformed by the use of synchrotron radiation. In the mid-1960's the 180 MeV electron synchrotron at the National Bureau of Standards, Washington, DC, was used to discover many resonances in the photoionization continua of atoms and simple molecules. The resonances were characterized in terms of the excited states involved, their energies and lifetimes. This article concentrates on that period. As dedicated high-flux storage rings became available, the emphasis turned to the study of the products of the photoionization process in order to further understand the electron correlation effects that had been uncovered earlier; examples of these more sophisticated experiments are given.

Keywords: photoionization; atomic and molecular physics, early years.

1. Introduction

Synchrotron radiation was first observed some 50 years ago but the first experiments were performed by Tomboulian & Hartman (1956) at Cornell ten years later. In 1961 the National Bureau of Standards (NBS), in Washington, DC, modified its 180 MeV electron synchrotron to allow access to the radiation. A substantial part of this article is devoted to the work undertaken in atomic and molecular physics at the NBS over a five-year period in the mid-1960's.

The NBS machine was truly a 'first-generation' source, with an average current of 0.1 mA and therefore the application of techniques such as photoelectron spectroscopy were not contemplated at that time. Subsequently, the NBS synchrotron was converted to a storage ring and some experiments using this 'second-generation' machine are described briefly. No attempt is made to provide a balanced view of the advances in our understanding of the atomic and molecular photoionization process made possible by the use of such powerful sources. Rather, this review looks back at a subset of experiments choosing Ar, Xe and O_2 as typical examples.

2. The situation prior to 1961

When asked to summarize a conference on vacuum ultraviolet (VUV) radiation physics, Weissler (1971) stated that "the tremendous advances in the field in the immediate post-war period started with the development of time-stable continuum light sources that were an improvement on the 'fickle' Lyman (1926) source". Nevertheless, when I joined the spectroscopy group at Imperial College in 1958, Garton had recently put together an experiment comprising a Lyman flash tube, a King furnace and a 3 m normal-incidence vacuum spectrometer. The aim was to study the absorption spectra of atoms below 2000 Å. The emission spectra of many atoms had been published by this time and one of the aims was to aid spectral analysis by picking out those lines that involved transitions to the ground state.

Pioneering work on the VUV absorption spectra of atoms was performed in the 1930's by Beutler in Berlin. Since facilities at that time were relatively poor, he had concentrated on the inert gases Ar, Kr and Xe and the more easily vapourizable atoms such as Hg and the alkalis. Our aim was to study the less vapourizable atoms. However, efforts were initially concentrated on the alkaline-earth elements Mg, Ca, Sr and Ba. Those familiar with the history of atomic theory will recall that the interpretation of the spectra of these 'two-electron' atoms played a crucial role in its development.

The absorption spectra of Ca, Sr and Ba exhibited many broad features associated with doubly excited states. The breadth of these lines is due to the process of autoionization, a rapid ($\sim 10^{-14}$ s) radiationless decay into the adjacent continuum. (The fact that these excited states decay so rapidly is the reason why they cannot be seen in an emission spectrum.) Some of the absorption lines exhibited very asymmetric profiles but it had been known since the time of Beutler that lines broadened by autoionization were often decidedly asymmetric. In fact, one or two 'window' resonances were observed but were not recognized as such (see later discussion). In Ca, for example, many of the two-electron excitations of the type $3dnf$ (where $n = 4, 5, \ldots$) were observed approaching the $3d$ state of Ca^+ in the limit. Since the ground state of Ca is $4s^2\ ^1S_0$, the transitions involved $\Delta l_1 = 2$ and $\Delta l_2 = 3$, transitions totally forbidden in

the context of the conventional $\Delta l = 1$ selection rule (see Garton & Codling, 1965).

One of the problems at that time was the lack of a 'pure' continuum source. To obtain a reasonably high black-body temperature the Lyman source had to be pulsed and this meant that many emission lines from highly ionized species were superimposed on the continuum. If one of these emission lines happened to fall on top of an absorption feature, the feature could be missed entirely. Moreover, sputtered electrode and wall material tended to coat either window, pre-mirror or entrance slit. Garton (1959) himself developed a pulsed source of continuum, the Garton flash tube, that was a great improvement in terms of shot-to-shot fluctuations and sputtered material but it was by no means perfect.

During early 1961, Branscomb, the head of the Atomic Physics Division at the National Bureau of Standards, Washington, DC, visited Garton's Laboratory. The NBS were intending to modify its 180 MeV electron synchrotron in order to make use of the synchrotron radiation. There was a position available for two years and I had the experience they required.

3. The National Bureau of Standards (1961–1966)

I joined the NBS on 1 September 1961 at the same time as Dr Robert P. Madden. Together with Russell Johnson we constituted a new section within the Atomic Physics Division, 'Far Ultraviolet Radiation Physics'. The first tasks were to build a Garton flash tube, to focus a new normal-incidence 1 m McPherson monochromator and to learn about the characteristics of synchrotron radiation. It appeared that the theory of synchrotron radiation was well developed (see Codling & Madden, 1965*a*, and references therein), and that the radiation was first observed by Elder, Gurewitsch, Langmuir & Pollock (1947).

One obvious reason for the interest of the NBS in synchrotron radiation was that it ought to provide a fundamental standard of flux for the VUV spectral region. Indeed, in an all-too-brief period of access to the Cornell 300 MeV electron synchrotron, Tomboulian & Hartman (1956) conducted experiments that showed conclusively that synchrotron radiation could be used as an intensity standard and, perhaps more importantly, as a new source of continuum for the VUV. They cast the theory developed by Schwinger (1949) into a more convenient form and this was used to calculate the angular and spectral distributions to be expected from the NBS 180 MeV machine.

Such curves are now very familiar but at the time it was surprising to find that if one wished to work in the 100–600 Å region (the lower wavelength limit was defined by the 180 MeV energy), then the NBS machine, with its radius of 0.84 m, was much superior to the 6 GeV 26 m Cambridge synchrotron, assuming, of course, identical beam currents. The latter machine had been specifically designed to reduce the loss mechanism (synchrotron radiation), hence the large radius.

Since the synchrotron was a potential radiometric standard of flux for the VUV, it was important to check to what extent the angular distributions and states of polarization calculated for a single electron in circular orbit were applicable in a real situation, with many electrons in somewhat different orbits, subject to radial and vertical oscillations. The radiation had been studied experimentally but only one attempt had been made to obtain data using photoelectric detection (Joos, 1960). The results indicated a considerable asymmetry in the angular distribution of the radiation for both vertical and horizontal polarizations.

In 1961 the NBS synchrotron was modified by adding a single tangent port, so that the radiation could be accessed. A view of the modified donut is shown in Fig. 1, with the tangent port at the top right and the pumping system at the bottom. As in all early work using synchrotron radiation the spectroscopists were to be parasitic users. The first experiments at NBS, a series of pinhole pictures, indicated that the cross section of the electron beam was elliptical, with a major-to-minor axis ratio of ~2:1. The vertical electron-density distribution was Gaussian, with a halfwidth of ~1 mm. This allowed a critical comparison between experiment and theory.

The NBS synchrotron utilized a 60-cycle sinusoidal magnetic field, the electrons being injected at zero field and reaching peak energy at the peak of the magnetic field. By appropriate gating and manipulation of parameters it was possible to limit the electron energy spread to less than 1%.

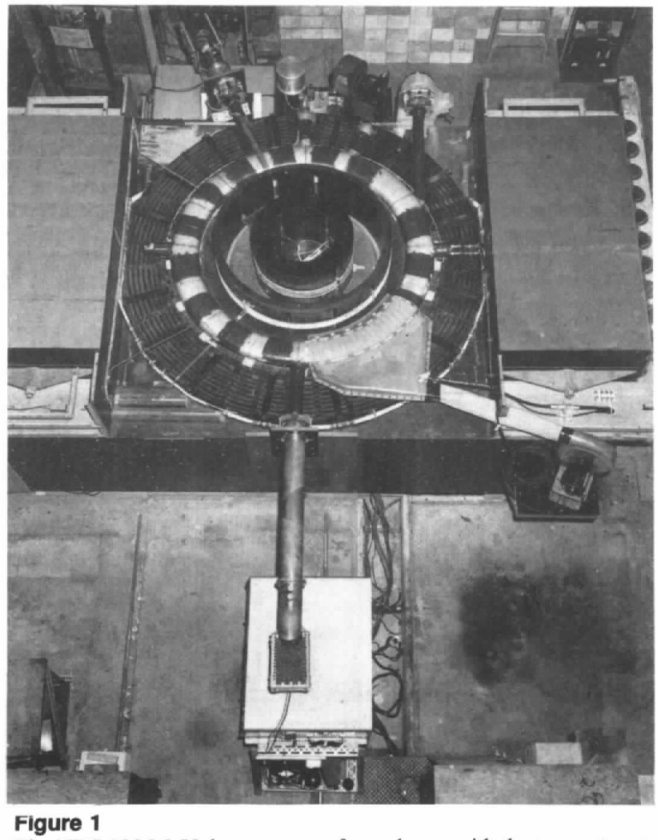

Figure 1
The NBS 180 MeV donut as seen from above, with the tangent port to the top right.

Using photoelectric detection the angular distribution and the state of polarization of the radiation were determined. The agreement between experiment and theory was quite impressive (Codling & Madden, 1965*a*). In particular, the radiation was completely symmetric with respect to the orbital plane and almost 100% linearly polarized in the orbital plane.

It was of further interest to test that the two components were exactly 90° out of phase. Using a quarter-wave plate the classical test for 90° phase retardation was conducted. Within the limits of experimental error (~5%) the correct phase relationship was observed. The radiation became more circularly polarized as one moved further off axis with the sense of circular polarization (left or right) changing, depending on whether one was above or below the orbital plane.

Finally, it was important to determine the number of electrons in the beam. The synchrotron radiation output was compared with the output of a calibrated tungsten lamp, assuming the Schwinger theory to be correct. At 180 MeV there were no more than 10^8 electrons per pulse in orbit. This corresponds to an average current of ~0.1 mA. Knowing this average current one could estimate the number of photons that would fall on the entrance slit of a spectrometer placed at a certain distance from the tangent point and make a rough estimate of exposure times required.

Whilst these experiments were underway, a 3 m grazing-incidence Rowland-circle spectrograph was under construction at the NBS. It was designed to withstand, without loss of resolution, the strong vibrations and large temperature changes in the close vicinity of the synchrotron. As is well known, the resolution of such an instrument is slit-width-limited and therefore, using a grating with 600 lines mm^{-1}, a resolution of 0.06 Å should be achieved using a 10 μm slit. By constructing the spectrograph in a single material and eliminating all non-essential adjustments, the resolution achieved was very close to this theoretical value.

One further reason for achieving such a high resolution was the method of alignment, whereby the entrance slit, grating and Rowland rail (on which the photographic plate sat directly) were located on the Rowland circle to high accuracy using a swinging arm (see Madden, Ederer & Codling, 1967). Because of the accuracy of location of the various components on the Rowland circle, it was possible to use the grating equation and measurement of the position of spectral features along the circle, that is along the photographic plate, to determine wavelengths to an accuracy of ~0.01 Å.

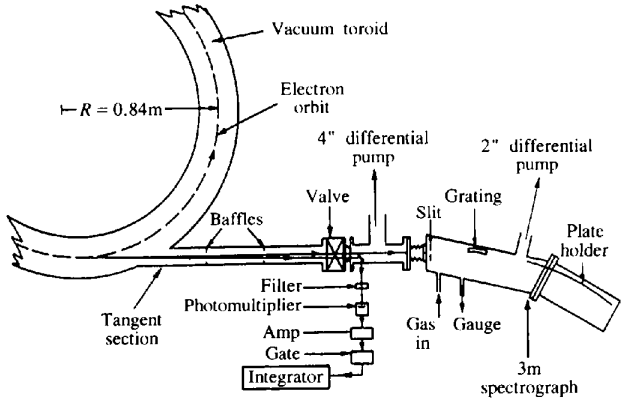

Figure 2
Experimental arrangement for photoabsorption spectroscopy.

3.1. *Atomic spectroscopy at the NBS*

In early 1963 the 3 m spectrograph was placed on line, with its entrance slit a mere 2 m from the tangent point! No light-collecting mirror was used to enhance the angular acceptance in the horizontal plane, since the modest gain that would have accrued by matching to the *f*-number of the spectrograph would have been decreased, to some extent, by the poor reflectivity of the mirror. The experimental arrangement is shown schematically in Fig. 2. Using the entrance slit as a stage of differential pumping, the spectrograph itself could be used as the absorption cell. A mirror intercepted part of the beam and fed it to a photomultiplier and integrator to provide an exposure time. Although the measurement of circulating current had allowed an estimate of the flux that would fall on the 10 μm entrance slit, and therefore the exposure time that should be required, it was nevertheless encouraging to find that the estimate of minutes rather than hours was correct.

Because of the form of the grating equation and the fact that a pure continuum source was being used, there could be problems of high-order overlap. In the case of He discussed below, the problem did not occur because the 100 Å second-order radiation from the NBS machine was quite weak. In other cases, thin (~1000 Å) films of Al were used to remove overlapping orders in the 170–340 Å range. In fact, by inserting Al films into the beam, it was possible to determine the location of the $L_{II,III}$ edges to a greater accuracy than had been performed before (see Codling & Madden, 1968). A value of 0.43 eV for the spin-orbit splitting compared well with the $K\alpha_1$–$K\alpha_2$ splitting determined by Nordfors (1955). Having access to a pure continuum highlighted, for the first time, the effect that absorption edges could have on the reflectivity of a diffraction grating. The Al-coated grating used in the 3 m spectrograph introduced reflection anomalies in first, second and third order at 170, 341 and 512 Å.

The first gas that was leaked into the spectrograph was He, this being the simplest two-electron atom. One expected to see structure associated with two-electron excitation in the 200 Å (60 eV) region. There was evidence of structure at 60 eV in the early electron-loss spectra of Whiddington & Priestley (1934) and more recently Silverman & Lassettre (1964). The resolving power in the synchrotron experiment was expected to be about a factor of 20 better and therefore one anticipated seeing much more structure. In the event a single series of resonances was seen; this is shown at the top of Fig. 3 (see Madden & Codling, 1963). (The photograph is a positive print and therefore black denotes absorption.) The He spectrum between 200 and 170 Å will be discussed in more detail below. However, one sees in both the He and Ne spectrum a series of resonances with decidedly asymmetric

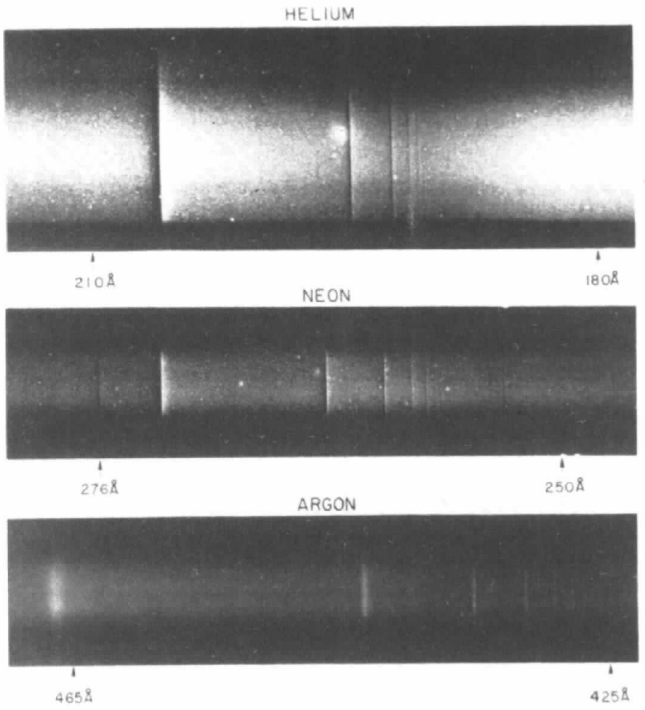

Figure 3
Resonances in the photoionization continua of He, Ne and Ar. Increasing blackness denotes increasing absorption (from Madden & Codling, 1963).

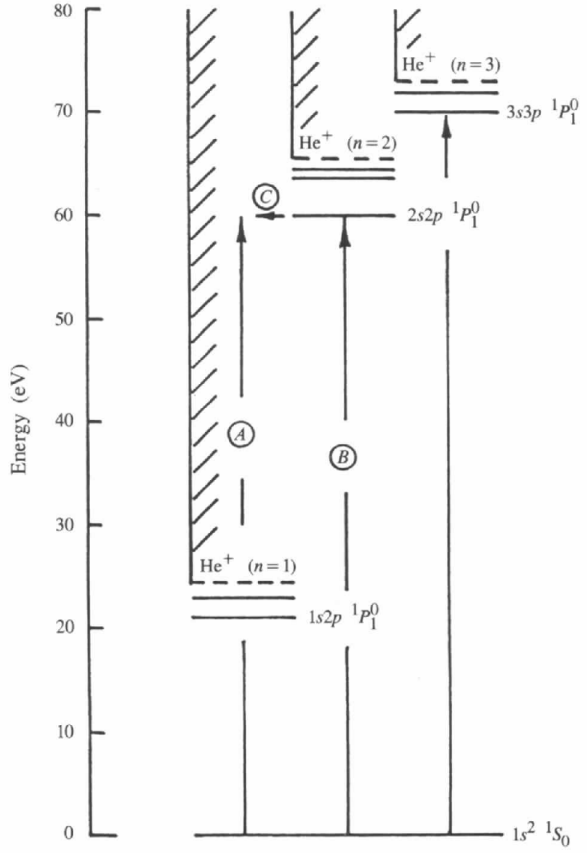

Figure 4
A simplified energy-level diagram of He, showing ground-state transitions to the continuum (*A*), to the quasi-discrete state (*B*) and the autoionization process (*C*).

profiles. These resonances were said to have 'Beutler–Fano' profiles, in recognition of the early work of Beutler (1935) and Fano (1935).

The Ar resonances in Fig. 3, on the other hand, have the appearance of a series of emission lines and their observation would have been more surprising than it was were it not for the then recent work of Fano (1961). What one is observing are discrete lacks of absorption. These resonances, which became known as 'window' resonances, are characterized by a low value of the line-shape parameter, q (see below). As mentioned earlier, others had observed these unusual profiles without appreciating their significance. Indeed, in one case it was thought that they were emission lines emanating from the background continuum source (see Hopfield, 1930*a*). The series of resonances in Ne and Ar were said to be 'probably' due to excitation of subshell $2s$ and $3s$ electrons, although in retrospect it is hard to see what else they could have been.

The spectrum of He, Fig. 3, was of fundamental importance because doubly excited states of He provide the simplest possible three-body system (apart from H^-) in which to study electron correlation effects. These doubly excited states autoionize; this process is explained briefly in Fig. 4, a simplified energy-level diagram of He. The processes of importance are:

(*A*) photoionization: $He + h\nu \rightarrow He^+ + e$,

(*B*) double excitation: $He + h\nu \rightarrow He^{**}$,

(*C*) autoionization: $He^{**} \rightarrow He^+ + e$.

Clearly, process (*B*) can only occur at specific energies, for example 60.1 eV in the case of the $2s2p\ ^1P_1$ excited state. The lifetime of such a state is very short, typically 10^{-13}–10^{-14} s, before process (*C*) occurs. The fact that both processes (*A*) and (*B*)–(*C*) leave the system in the same final

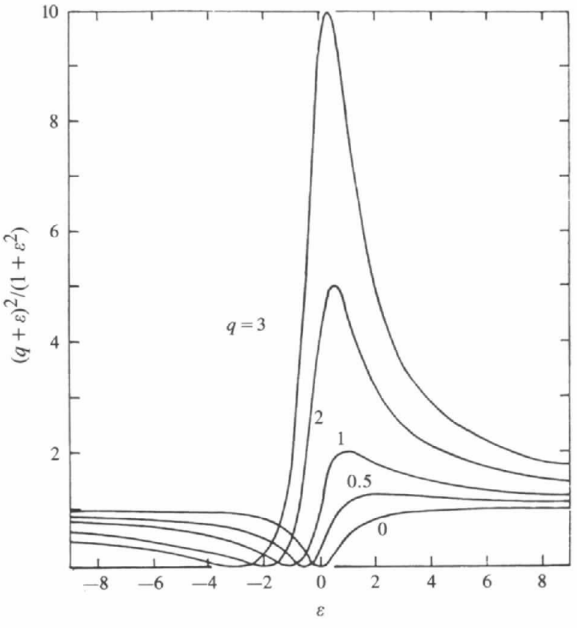

Figure 5
Theoretical curves of the variation of absorption cross section in the region of a resonance, normalized to 1 in the far wings (from Fano, 1961).

state means that interference can occur, leading to the asymmetric resonances observed in Fig. 3.

In this simplest of examples of configuration interaction, involving a single discrete state and a single set of continuum states of identical parity, the $1sEp$ states, the absorption cross section in the region of the resonance is given by Fano (1961) as:

$$\sigma = \sigma_A(q+\varepsilon)^2/(1+\varepsilon^2), \qquad (1)$$

where σ_A is the cross section in the wings, ε is the photon energy in units of the halfwidth of the resonance, Γ, and q is the line profile index, involving matrix elements associated with processes (A), (B) and (C). A set of curves of the variation in cross section is shown in Fig. 5 for various values of q (see Fano, 1961). Reversing q reverses the sense of the asymmetry (the zero cross section occurs at $q = -\varepsilon$). Note that when $q = 0$ the cross section shows only a decrease; one observes a window resonance.

As mentioned above, the He spectrum was of fundamental importance because one is observing a three-body system, unencumbered by additional potentially interacting electrons. When the spectrum was first obtained, one had expected to observe two series approaching the $n = 2$ ($2s$ and $2p$) state of He^+ as the limit, labelled $2snp\ ^1P_1$, and $2pns\ ^1P_1$, having a common first member $2s2p\ ^1P_1$. However, it soon became clear to Cooper, Fano & Prats (1963) that these two series should mix strongly and that there should indeed be two series, but one would be strong, the other extremely weak. The two series of excited states were described as follows:

$$\psi(sp, 2n\pm) = [U(2snp) \pm U(2pns)]/2^{1/2}. \qquad (2)$$

The series labelled $(sp, 2n+)$ would be strong, the series labelled $(sp, 2n-)$ would be weak. Thus, experiment (Fig. 3) and theory were reconciled.

This raised the question as to the conditions under which the weaker series might be observed. Theory suggested that

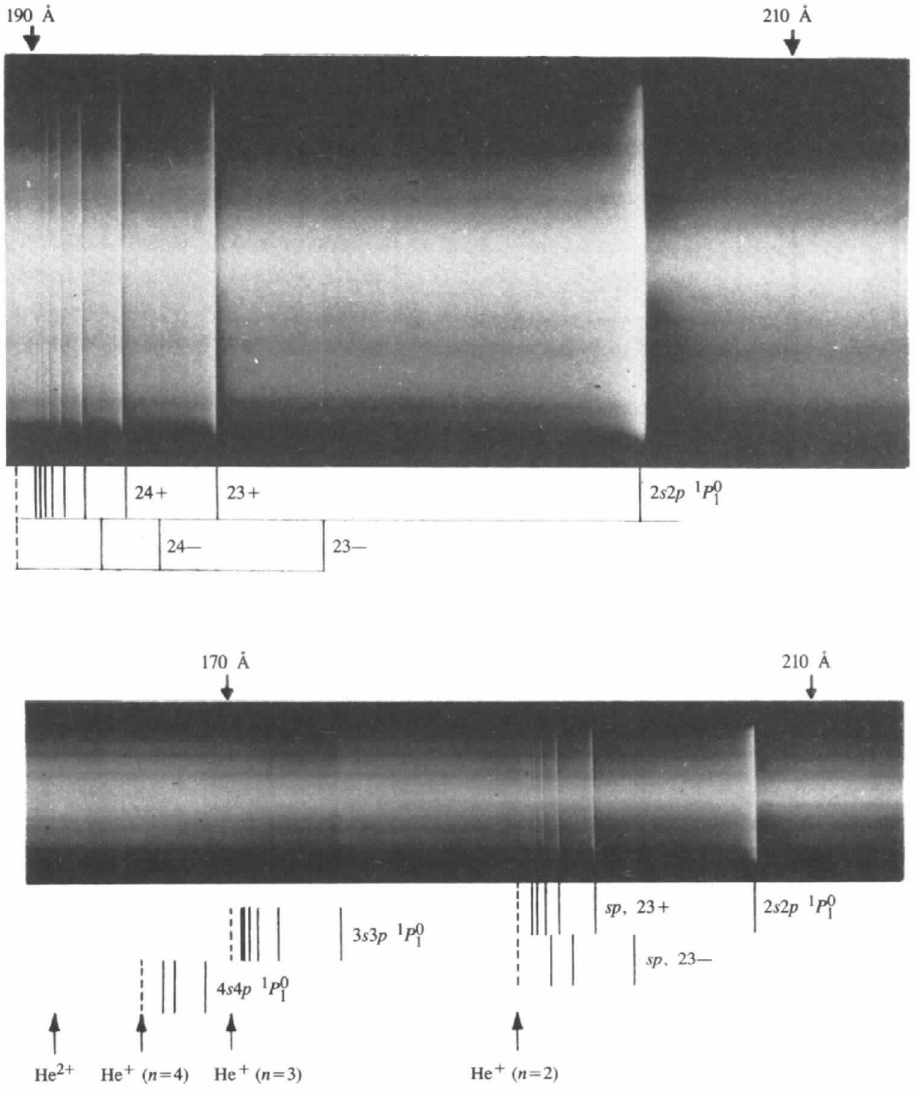

Figure 6
The absorption spectrum of He between 160 and 215 Å, showing four series of resonances. The enlarged portion (above) shows the weak $(sp, 2n-)$ series (from Madden & Codling, 1965).

the '−' series should be two orders of magnitude weaker than the '+' series and extremely difficult to see. In fact, the use of a new less-grainy batch of photographic plates led immediately to observation of the weaker series. Three members of the series could be seen and they had the same profile (*i.e.* negative q value) as the stronger series. The first of these can be seen in the upper spectrum of Fig. 6. Two additional series of resonances were discovered at the same time; the (sp, $3n$+) and (sp, $4n$+) series approaching the n = 3 and n = 4 states of He^+ in the limit. These series can just be seen in the lower spectrum of Fig. 6.

Although there are undoubtedly limitations in the photographic technique, there are some advantages. For example, in the lower spectrum one sees the entire region of interest in one picture and the human eye is very good at picking out structure. One immediately sees (i) the large difference in oscillator strength of the '+' and '−' series, (ii) the reversal in sign of q for the (sp, $3n$+) series compared with the (sp, $2n$+) series, and (iii) the lack of contrast (visibility) of the (sp, $3n$+) series compared with the (sp, $2n$+) series. From densitometer traces of the broadest resonances one could estimate their width and therefore their lifetime against autoionization.

The $2s2p\ ^1P_1$ resonance was of such theoretical interest that its profile was studied in detail, photographically. The problem of the variability of the sensitivity from one photographic plate to another was avoided by using a density coincidence technique. This technique also removed the problem of non-linearity of the photographic emulsion (see Madden & Codling, 1965). Advantage was taken of the strongly directional property of synchrotron radiation to take two exposures on one plate using an occulter. (Normally, astigmatism turns a point on the entrance slit into a line on the photographic plate.) Firstly, spectra were taken, without He, at two settings of the occulter and their exposures adjusted to give equal densities across the wavelength range of interest. A second pair were then taken at these same settings, one of which was taken while He filled the spectrograph to a known pressure. Again, the exposure times were adjusted to produce equal density at a particular point within the resonance profile. This procedure, whilst tedious, allowed absorption coefficients, or photoionization cross sections, to be determined absolutely.

Fig. 7 shows the results for the $2s2p\ ^1P_1$ resonance. The solid curve represents the best fit of the data to a resonance profile of the form given in equation (1). One sees that the parameters, q and Γ, are quoted to an accuracy of ~10%. An interesting aspect is that the cross section falls to zero at a particular point in the resonance, as predicted when a single resonance interacts with a single set of continua. From the halfwidth, an autoionization lifetime of 1.7×10^{-14} s was obtained. This agreed with an early calculation by Burke, McVicar & Smith (1963). The location of the resonance peak at 60.12 eV also agreed well with theory.

The labelling of the main series of resonances as an admixture of $2snp$ and $2pns$ neglected the influence of another channel, $2pnd\ ^1P_1$. Burke *et al.* (1963) calculated the position of these resonances, but no additional structure could be found with the resolution available at the time ($E/\Delta E \simeq 3500$). It is interesting to note that it took almost 30 years for the $2pnd$ series to be observed with the SX700/II monochromator at BESSY (Domke, Remmers & Kaindl, 1992) with a resolution of ~16 000. Even more recently, the Advanced Light Source at Berkeley has been

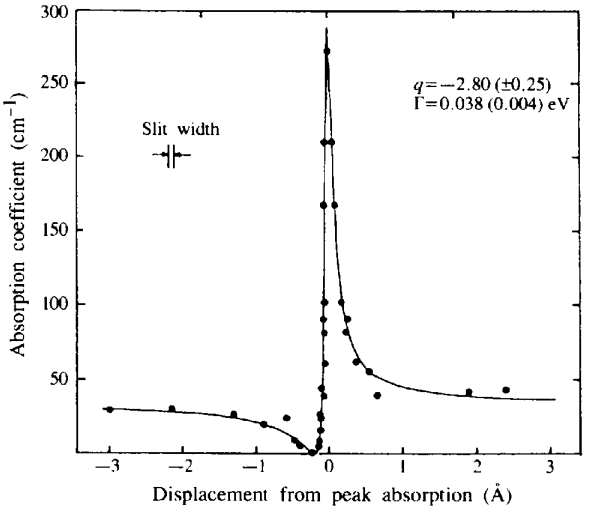

Figure 7
The absorption cross section of He in the region of the $2s2p$ resonance. The solid curve is the best fit to the data with the parameters given in the figure.

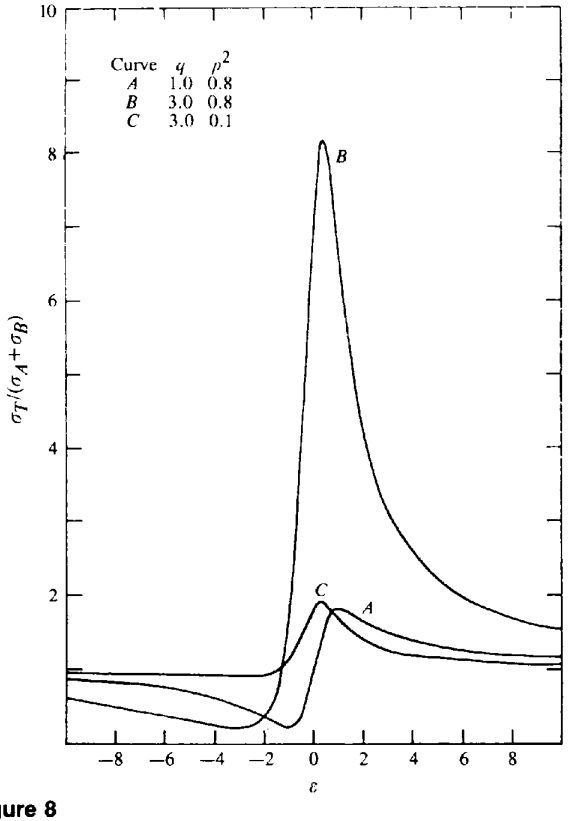

Figure 8
A plot of three resonance profiles, showing the effects on the line shape of varying q and ρ^2.

used to observe many more resonances, using a resolution of ~50 000.

It was pointed out earlier that the (sp, $3n$+) series had a much lower contrast than those approaching the $n = 2$ limit. This can be explained in terms of a simple generalization of equation (1):

$$\sigma_T = \sigma_A(q + \varepsilon)^2/(1 + \varepsilon^2) + \sigma_B. \quad (3)$$

Here we separate the total cross section into two contributions; the continua (σ_A) that do interact with the discrete state and those that do not (σ_B). Fano & Cooper (1965) introduced a parameter, ρ, the autoionization-to-dipole correlation coefficient or overlap integral, relating to σ_A and σ_B in the relationship:

$$\rho^2 = \sigma_A/(\sigma_A + \sigma_B). \quad (4)$$

The overlap is that between the final-state wave function reached by autoionization and that reached by direct photoionization.

The curves in Fig. 8 show the effects of both increasing the profile index, q, at constant ρ^2 and decreasing ρ^2 at a constant q. When ρ^2 is small, the resonance appears as a conventional absorption line with little apparent asymmetry, even though q is quite large. In the case of the (sp, $3n$+) series in He, Fig. 6, the low contrast (low ρ^2) is a result of the fact that this state can in principle interact with two continua, $1sEp$ and $2sEp$ ($2pEs$), but interacts strongly with the latter, which is only a small fraction of the total. Assuming pure L–S coupling, the value of ρ^2 for the $2s2p\ ^1P_1$ resonance is unity and was found experimentally to be so (see Fig. 7). At one point in the resonance the absorption cross section is zero.

In Ne (Codling, Madden & Ederer, 1967) the strongest asymmetric resonance at 272 Å, Fig. 3, is due to the one-electron transition: $2s^22p^6\ ^1S_0 \rightarrow 2s2p^63p\ ^1P_1$. Here, the discrete state can interact with five $J = 1$ continua and the parameters obtained are $q = -1.6$ and $\rho^2 = 0.70$. The excess oscillator strength, f, could be determined from the formula of Fano & Cooper (1965):

$$f = k(\sigma_A + \sigma_B)\pi\Gamma\rho^2(q^2 - 1). \quad (5)$$

One sees that the excess oscillator strength is proportional to $(q^2 - 1)$, and when $q = 1$ there is no excess (see Fig. 5). Furthermore, theory suggests that within an unperturbed Rydberg series the values of q and ρ^2 should remain constant.

When considering the family of curves in Fig. 8, two cases are of particular interest. When $q >> 1$ (and usually ρ^2 is small) the asymmetry is no longer observed. The absorption profile tends to the conventional Lorentzian shape. Examples of such symmetric resonances are seen in Xe in the 190 Å region and in Kr in the 135 Å region. Fig. 9 shows the absorption spectrum of Xe from 80 to 190 Å. The structure around 180 Å is associated with two series of resonances approaching the $4d^{-1}(^2D_{3/2})$ and $4d^{-1}(^2D_{5/2})$ states of Xe^+. Extrapolating these series to their limits allowed the binding energy of the $4d$ electron in Xe to be determined for the first time (see Codling & Madden, 1964).

At the time of their discovery it was not understood why four series of resonances were not observed, two to each limit, $4d \rightarrow nf$ and $4d \rightarrow np$. The $4d \rightarrow nf$ series ought to have been the stronger of the two but from the quantum defects of the excited states it was clear that the series involved excited p electrons and that the $4d \rightarrow nf$ series were entirely missing. At about that same time, Ederer (1964), working with Tomboulian at Cornell, studied the absorption of Xe in the region below 200 Å. He found a broad feature centred around 120 Å (see also Fig. 9), which was associated with a centrifugal barrier phenomenon. In fact, the lack of observation of the $4d \rightarrow nf$ series and the broad feature in the continuum stem from the same source. Only when the continuum f electrons have sufficient energy (15 eV and above) to overcome the centrifugal barrier can there be substantial overlap with the ground-state wave function and therefore a large absorption cross section.

It is interesting to note that in the case of He, Ne and Ar the series of resonances can be seen to high-series members (almost 20 in the case of Ar), until the resolving power is no longer sufficient. This is because the autoionization process produces resonances whose widths reduce at roughly the same rate as the distance between resonances. In the case of the $4d \rightarrow np$ series in Xe, however, only four or five

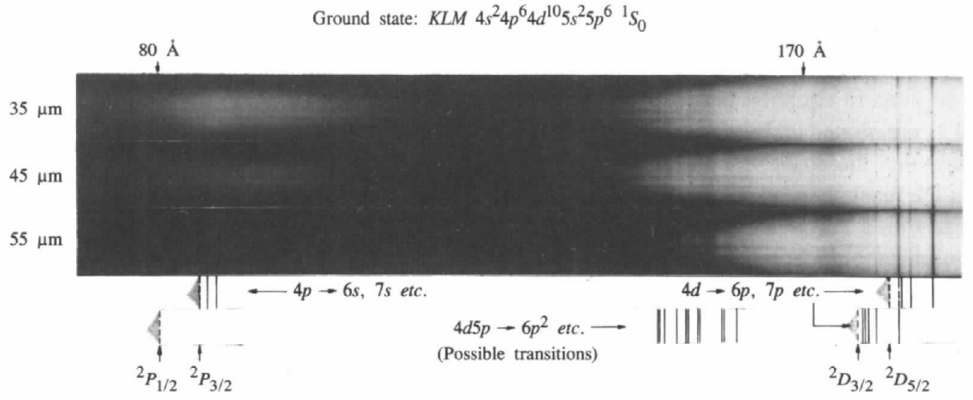

Figure 9
The absorption spectrum of Xe in the 80–190 Å region, at three different Xe pressures (from Codling & Madden, 1965*b*)

resonances are seen. This is because the width of the series of resonances is roughly constant at high n, but the resonances close up rapidly and hence they merge. It was assumed that what one was observing here was the Auger effect rather than autoionization. The excited electron ($7p$, $8p$ *etc.*) becomes a spectator to the Auger rearrangement of the core, with a constant lifetime and constant width.

There are, incidentally, two high-q resonances in the 90 Å region, associated with the excitation of the $4p$ electron to $6s$ and $7s$ orbitals. This observation allowed an estimate to be made of the binding energy of the $4p$ electron of 145.6 (±0.5) eV. The fact that no resonances appeared to approach the $^2P_{1/2}$ limit was explained in terms of rapid Auger decay into the newly opened $^2P_{3/2}$ channel (see Codling & Madden, 1965*b*).

The inert gases have provided many interesting examples of autoionization structure in their absorption spectra; the heavier the inert gas, the more complex the spectrum. In many cases only the higher members of the Rydberg series could be picked out and classified with certainty, since the series approached excited states of the ion that were usually known from analysis of their emission spectra. Many examples of configuration mixing were uncovered, but the analysis was hindered by the lack of any real theoretical input. Nevertheless, the energies and character (line shapes) of the various resonances were catalogued (see, for example, Codling & Madden, 1972). These resonances were subsequently used as internal standards for electron energy-loss experiments; these electron energy-loss experiments could access optically forbidden as well as allowed transitions.

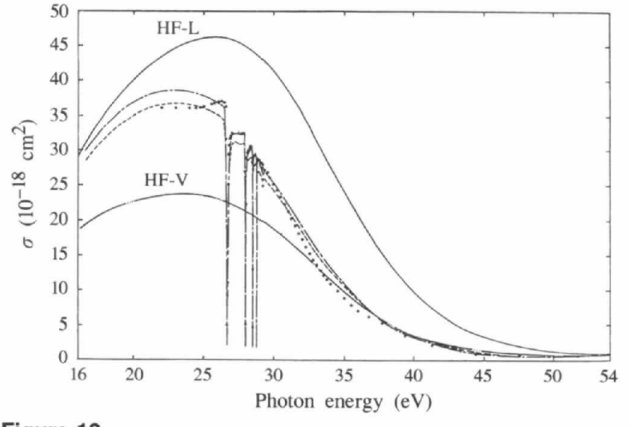

Figure 10
The photoabsorption (photoionization) cross section of Ar in the 16–54 eV energy range (770–230 Å). The circles are the data points of Madden *et al.* (1969), the theoretical curves are from Kelly & Simons (1973). HF-L and HF-V refer to the Hartree–Fock length and velocity forms, respectively.

Some of the electron excitations in Xe (KLM $4s^24p^64d^{10}5s^25p^6$) have been mentioned. Thirty five years ago only the absorption spectrum associated with excitation of the outer $5p$ electron was known. At the NBS, structures associated with the excitation of the following electrons were discovered: (i) the subshell $5s$ electron, (ii) two outer $5p$ electrons simultaneously, (iii) the $5s$ and $5p$ electrons simultaneously, (iv) the $4d$ electron, (v) the $4d$ and $5p$ electrons simultaneously, and (vi) the $4p$ electron.

We have seen, in the case of the $2s2p\ ^1P_1$ state of He, the difficulties in determining absolute cross sections and resonance profiles using the photographic technique. In 1964, a 3 m grazing-incidence monochromator was designed and built in-house at the NBS (Madden *et al.*, 1967), based again on the Rowland-circle geometry. The monochromator was designed to achieve a slit-width-limited resolution of 0.06 Å and have a wavelength range from 620 Å downwards. A bellows seal at the entrance slit restricted the gas flow from the monochromator. The detector, an open multiplier, was maintained at good vacuum using a viton diaphragm and telescopic tubes. The alignment procedure was identical to that used for the spectrograph and the resolution achieved was almost identical.

The monochromator was first used with Ne, to obtain absolute cross sections and resonance parameters (q, Γ and ρ^2) for the two-electron excitation state $2p^4\ (^3P)\ 3s3p\ ^1P_1$ at

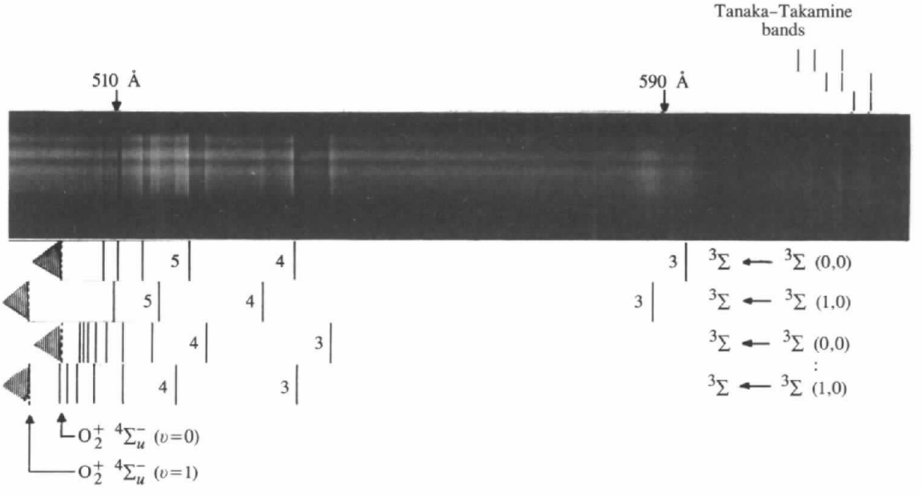

Figure 11
The absorption spectrum of O_2 in the 500–625 Å region, showing four Rydberg series (from Codling & Madden, 1965*c*).

276 Å and the first three members of the $2s2p^6np\ ^1P_1$ series, in the range 272–260 Å (see Fig. 3). The absorption-like appearance of the first resonance is reflected in the low correlation coefficient obtained, $\rho^2 = 0.17$. The following three resonances, with $n = 3$, 4 and 5, were found to have exactly the same q value (−1.6) and ρ^2 (0.70), within experimental error. The resonance widths varied as the inverse cube of the effective quantum number, n^*, as predicted for an unperturbed Rydberg series. The continuum cross section associated with the one-electron series (or channel) was found to be only 0.5% of the pre-existing continuum cross section. This highlights the fact that these resonances, although small in absolute oscillator strength, are nevertheless quite easy to see because of their asymmetric profiles.

The monochromator was subsequently used to determine the absolute cross section for Ar in the region 20–35 eV (see Madden, Ederer & Codling, 1969). Fig. 10 shows the series of window resonances previously seen in Fig. 3, associated with excitation of the subshell 3*s* electron. The first three resonances were studied and the parameters q, Γ and ρ^2 obtained. Once again, the values of q (0.20) and ρ^2 (0.85) were the same, within experimental error, and the product $n^{*3}\Gamma$ was constant. In the case of such low-q resonances, the excess oscillator strength is negative. However, when the discrete state interacts with a large fraction of the available continua, the excess oscillator strength is a poorly defined quantity. Not long after these data were published, Kelly & Simons (1973) used a many-body perturbation theory approach to calculate the photoionization cross section in this region. They included intrachannel and interchannel interactions as well as the effects of virtual double excitations, and their cross sections were in excellent agreement with the experiment, even to the extent of describing the discrete resonances.

3.2. *Molecular spectroscopy at the NBS*

In molecules, as in atoms, the first experiments involved taking spectra with the 3 m spectrograph below 620 Å. Fig. 11 is the absorption spectrum obtained for O_2 in the region 620–500 Å. The new bands (resonances) observed by Codling & Madden (1965*c*) were quite weak relative to the continuum absorption on which they were superimposed. It is interesting to note that, although the Lyman continuum source had long been available for absorption studies in this spectral region, the system had not been reported. Presumably the combination of a relatively weak system and a source with many unwanted emission lines superimposed prevented earlier observation of this structure. The high-series members of the Tanaka & Takamine (1942) bands are clearly observed on the right of the figure. We were unable to obtain highly accurate measurements of the high-series members of the series but were able to confirm the location of the $v = 0$, 1 and 2 levels of the $^2\Sigma_g^-$ state of O_2^+ to which the series were converging in the limit.

Many of the newly observed absorption features are seen to have 'Beutler–Fano' profiles with both positive and negative values of q. Of particular interest were the two window resonances at about 590 Å; these will be discussed later. The wavelengths of the resonances were determined by introducing both O_2 and He into the spectrograph and using the well known wavelengths of the He principal series. The majority of the resonances could be fitted into four series, as shown below the figure. This analysis suggested that a new state of O_2^+ had been discovered, with its lowest vibrational state at 24.563 eV, and first vibrationally excited state at 24.754 eV.

However, Leblanc (1963) had recently analysed the Hopfield (1930*b*) emission bands of O_2 observed in the 1900–2400 Å region. These bands were initially assumed to be due to transitions in O_2, but rotational analysis of the bands led Leblanc to conclude that they were most probably due to transitions in O_2^+, with the lower electronic state being the $b\ ^4\Sigma_g^-$ state at ~18 eV. He tentatively classified the upper state as $^4\Sigma_u^-$ and predicted that the state would lie 24.56 eV above the ground state of O_2. The situation is depicted in Fig. 12. To the right are given the electron configurations. Although the electron configuration of the $c\ ^4\Sigma_u^-$ state was not given by Leblanc, the state was most likely to be associated with the removal of the $\sigma_u 2s$ electron.

The four series observed in Fig. 11 could therefore be associated with the Rydberg series approaching the c state of O_2^+. The two strongest series were assumed to approach the $v = 0$ level, the two weaker series the $v = 1$ level. The vibrational spacing of 0.19 eV was close to that of the ground state of O_2 and the fact that a third series of resonances was not observed, even weakly, suggested an

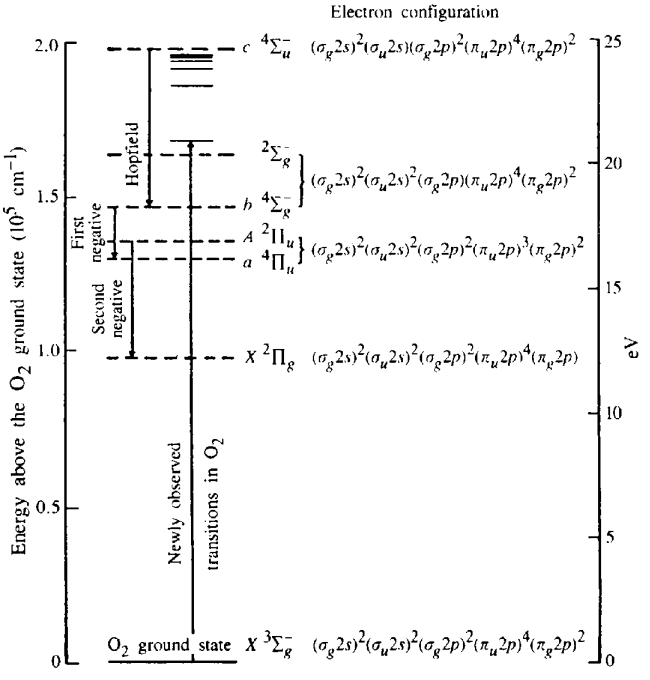

Figure 12
Energy levels of the O_2^+ molecular ion (dashed lines). The transitions in the O_2^+ ion are shown as downward arrows. The (then) newly observed Rydberg states of O_2 are shown as horizontal lines.

equilibrium internuclear separation for the c state that was quite similar to that of the ground state of O_2. The real reason for this lack of observation of a series to the $v = 2$ level, rapid tunnelling, was not appreciated until much later; see §4.

The diatomic molecules N_2 and CO were also introduced into the spectrograph but the structure observed was disappointingly weak. [The NO molecule was not introduced because it was thought that it might attack the Al grating. Subsequently, interesting structure was discovered by Narayama & Price (1972).] Both N_2 and CO showed vibrational features between ~500 and 600 Å. In the case of N_2 it appeared that these features must be associated, in the limit, with the known $C\ ^2\Sigma_u^+$ state of N_2^+ (Gilmore, 1965) lying at ~24 eV, but at that time is was impossible to definitively associate each feature to a specific vibrational state of the neutral (see Codling, 1966*a*).

The C state of N_2^+ was thought to be due to the simultaneous excitation of a $\pi_u 2p$ electron and removal of an outer $\sigma_g 2p$ electron, but there was considerable configuration mixing between the $B\ ^2\Sigma_u^+$ and $C\ ^2\Sigma_u^+$ states of N_2^+. One assumed, therefore, that although the absorption structure was associated with the two-electron excitation process, $(\pi_u 2p)^3(\sigma_g 2p)(\pi_g 2p)\ ns\sigma$, that what allowed the Rydberg series to be seen was the admixture of the configuration where a single $\sigma_u 2s$ electron was excited. A similar problem of configuration mixing hampered the analysis of the CO absorption spectrum. The spectrum and an attempted analysis was not published until the photoelectron spectrum had been obtained using the He II 304 Å line [see Codling & Potts (1974), but see also a companion paper by Asbrink, Fridh, Lindholm & Codling (1974) and the recent article of Balzer *et al.* (1994)].

Before moving away from photographic measurements on molecules at the NBS, it is perhaps worth reiterating that discrete structure associated with autoionizing processes in the 20–150 eV range was disappointingly weak or non-existent. Since experiments were performed by leaking the gas into the spectrograph itself, reactive gases such as HI or HCl were not studied. Non-reactive gases such as CO_2 did not show structure. The only relatively large molecule studied, SF_6, did show vibrational structure in the 550–600 Å region, associated with the symmetric stretching mode of an excited electronic state of the molecule (see Codling, 1966*b*). Three window resonances were seen, forming a series that converged to a limit at 462 Å (26.83 eV) and it was pointed out at the time that this coincided with the appearance of the SF_2^+ ion observed in the electron-impact ionization of SF_6 at 26.8 (±0.3) eV (see Dibeler & Mohler, 1948).

In summary, the early photographic work at the NBS undoubtedly encouraged others to contemplate the use of synchrotron radiation as a source of pure continuum in the VUV spectral region. The photographic technique continued to be used for a few more years at the NBS. For example, the absorption spectrum of Li vapour around 200 Å was obtained by Ederer, Lucatorto & Madden (1970). This was a difficult experiment since conventional windows such as LiF could not be used to retain the vapour. A furnace based on the heat-pipe principle (Vidal & Cooper, 1969) was constructed and thin Al films were used to contain the essential buffer gas; the Al films also removed second-order and stray light. The column of inert buffer gas was restricted in length, since it too absorbed in the 200 Å region.

The Li atom was of fundamental theoretical significance, being next to He in the Periodic Table. The spectral features in the region 210–174 Å were associated with one- and two-electron excitations, $1s^2 2s\ ^2S_{1/2} \rightarrow 1s2snl$ and $1snln'l'$. The location of the resonances, such as $1s(2s2p\ ^1P)\ ^2P$, $1s(3s3p\ ^3P)^2P$ and $(1s2p\ ^1P)3s\ ^2P$, were in excellent agreement with the Hartree–Fock calculations of Cooper, Conneely, Smith & Ormonde (1970). The $1s^2 Ep$ continuum cross section was small at a distance of 50 eV above the first ionization limit and consequently the great majority of resonances appeared as simple absorption features ($q >> 1$).

4. After the NBS

The experiments discussed so far have dealt mainly with the discovery of 'fine' structure, *i.e.* discrete resonances, in the photoionization continuum of atoms and simple molecules using, for the most part, the photographic technique. The spectra provided accurate energies with which to compare theory. 'Gross' features in the continuum were also observed; for example, in Xe one saw a shape resonance at ~100 eV (see Fig. 9). Although rough estimates of absorption cross sections and oscillator strengths could be obtained, one required the use of photoelectric detection to obtain reliable data.

However, such data are of somewhat limited value, since the cross sections reflect the response of the system (the electrons) as a whole. If one wishes to study electron correlation effects such as intershell and intrashell interaction, one must perform more definitive experiments, where the *products* of the photoionization process are studied. That is, one must take photoelectron spectra, photoion spectra or fluorescence spectra. Such experiments, which require a greater experimental finesse and therefore greater photon flux, could not be performed easily on the first-generation synchrotrons, such as the NBS machine. However, when the NBS machine was converted, in 1974, to a storage ring (SURF II), such experiments became feasible.

There are many reviews on the use of these secondary techniques, both separately and in coincidence. In order to limit the scope of this article, the techniques described will generally be related to those atoms and molecules that have already been discussed. One fundamental requirement for these more complex experiments is a monochromator, rather than a spectrometer. Such a monochromator must provide photons of variable energy but *fixed direction*. This was quite straightforward in the spectral range above ~900 Å, because normal-incidence monochromators could be used. In the grazing-incidence regime, no 'constant-deviation' monochromators existed. Several designs were published,

some using the Rowland mounting, some using plane gratings, some toroidal gratings; some used the electron beam itself as the entrance slit (see Gudat & Kunz, 1979).

4.1. *Photoelectron spectroscopy*

Although the technique of photoelectron spectroscopy had been introduced by Siegbahn, Turner and Price in the early 1960's, it was not coupled with synchrotron radiation until the early 1970's. The principle of photoelectron spectroscopy, and the additional information it can provide, can be seen by returning to the Ar atom and the earlier Figs. 3 and 10. There we saw a series of window resonances approaching a limit at 424 Å (29.2 eV) and were able to parameterize the first three in terms of their q, Γ and ρ^2 values. However, having determined the cross section at 350 Å (35.4 eV), it was impossible to know in which state the Ar^+ ion had been left.

If a photon of this energy is incident on an assembly of Ar atoms, the Ar^+ ion may be left in its ground state ($3s^2 3p^5\ ^2P_{3/2}$), with the electron taking the excess energy of 19.6 eV, or in an excited state ($3s3p^6\ ^2S_{1/2}$) with the electron taking a much smaller energy of 6.2 eV. Fig. 13 shows the two possibilities. If the numbers of these electrons, *emitted into all angles*, can be determined, then the partial photoionization cross sections can be determined. In the early 1970's Lynch, Gardner, Codling & Marr (1973) measured the $3s$ partial cross section using the Glasgow 300 MeV synchrotron (0.1 mA average current). With such a low current the statistics were poor, although there were signs of a minimum in the cross section. Subsequently, the Daresbury NINA synchrotron was used to re-measure the $3s$ cross section; the results are shown in Fig. 14 (see Houlgate, West, Codling & Marr, 1976).

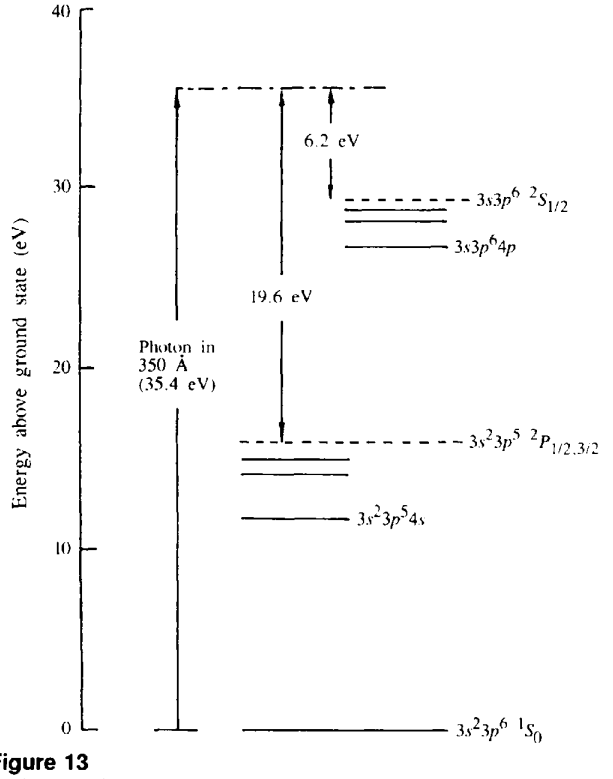

Figure 13
A simplified energy-level diagram of Ar, showing the principles of photoelectron spectroscopy of atoms. At a photon energy of 35.4 eV, two groups of photoelectrons are produced, with energies 6.2 and 19.6 eV.

At ~13 eV above threshold there is a zero minimum in the $3s$ cross section, which is not predicted by the Hartree–Fock calculation of Kennedy & Manson (1972). Calculations including intrashell interactions [correlation effects between the $3s$ and $3p$ electrons; see Burke & Taylor (1975)] show much better agreement with experiment. Amusia, Ivanov, Cherepkov & Chernysheva (1972) had earlier explained this minimum in terms of the screening of the $3s$ electrons from the incident electromagnetic wave by an antiphase oscillation of the $3p$ electrons. Note that the $3s$ cross section at threshold, ~1 Mb, is only a few percent of the total cross section and this small correlation effect could not have been seen in the total cross section.

One further example, this time of intershell rather than intrashell interaction, is seen in the region of the shape resonance in Xe at ~100 eV (see Fig. 9). Here is an example of inner-shell electrons influencing the behaviour of outer-shell electrons. In the single-electron picture it would be expected that the $5s$ and $5p$ partial cross sections would be monotonically decreasing at 100 eV. In fact, due to intershell interaction between the $4d$ electrons and the $5s(5p)$ electrons, the partial cross sections are enhanced (see West, Woodruff, Codling & Houlgate, 1976). The effect is shown in Fig. 15, where the random phase approximation with exchange (RPAE) calculations of Amusia, Ivanov, Cherepkov & Chernysheva (1974) are seen to predict the essential physics.

4.1.1. *Angular distribution of photoelectrons.* When attempting to determine partial cross sections for emission of electrons from specific subshells, one must either collect electrons over a full 2π solid angle or know the angular distribution of the electrons involved. In any event, a more searching test of theory is possible if one determines the

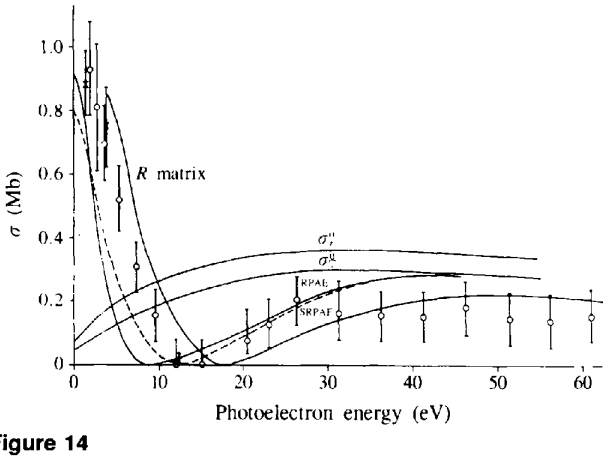

Figure 14
The partial photoionization cross section for removal of the Ar $3s$ electron (from Houlgate *et al.*, 1976). SRPAE refers to the simplified form of the random phase approximation with exchange approach.

angular distribution of photoelectrons. Using unpolarized radiation one can determine the angular distribution relative to the incident beam direction. However, with linearly polarized radiation one can determine the distribution relative to the direction of the E field. In this case the distribution is maximally anisotropic and the differential cross section is of the form

$$d\sigma_i/d\Omega = [\sigma_j(E)/4\pi][1 + \beta(E)P_2(\cos\theta)], \quad (6)$$

where σ_j is the partial photoionization cross section for channel j, θ is the angle between the electric vector and the direction of photoelectron emission, and $\beta(E)$ is the asymmetry parameter; $P_2(\cos\theta)$ is the second Legendre polynomial. In general, β is a complex expression involving angular momentum, l, partial wave phase shifts and dipole matrix elements (see Cooper & Zare, 1968). Bound electrons with s symmetry are ejected with a 'cosine-squared' distribution, *i.e.* $\beta = 2$. If the angular momentum of the atomic orbital has $l > 0$, the photoelectron may leave with angular momentum $l + 1$ and $l - 1$ and the interference between the two channels may result in a β that varies considerably with photon or photoelectron energy.

The Glasgow 300 MeV synchrotron was used for the first β measurements on the $3p$ electrons in Ar (see Mitchell & Codling, 1972). The radiation was dispersed by a 'constant-deviation' grazing-incidence monochromator (Codling & Mitchell, 1970) but the photoelectron signal was so weak that a spherical retarding potential electron spectrometer with a collection angle of 60° had to be used. Nevertheless, a considerable change in β with photoelectron energy was observed over the range 0–24 eV. Subsequently, data taken at the NINA synchrotron by Houlgate *et al.* (1976) confirmed this behaviour and extended the measurements to a photoelectron energy of 70 eV.

At threshold and well beyond, any contribution to the total cross section from the weaker $3p \rightarrow Es$ channel is masked by the much stronger $3p \rightarrow Ed$ channel. However, the interference between the two channels manifests itself in the form of a dramatic variation in β with photon energy. Of particular interest is the minimum at ~33 eV, or 50 eV photon energy, seen in Fig. 16. Here, there is a 'Cooper' minimum in the $3p \rightarrow Ed$ channel (Cooper, 1962); this is evidenced by the steady fall in cross section seen in Fig. 10. The remaining channel is $3p \rightarrow Es$, for which the electron angular distribution is isotropic and hence $\beta = 0$ in this region.

Inevitably, those early measurements of β were limited by the available photon flux. Once the second generation of sources, the dedicated storage rings, became available, it was possible to study the variation of β through a resonance. The bottom curve in Fig. 17 shows the variation in β on passing through the $3s3p^64p\ ^1P_1$ window resonance in Ar at 466 Å using the SURF II facility (see Codling, West, Parr, Dehmer & Stockbauer, 1980). The major variation in β, from 0.85 to 1.7, takes place within the width of the

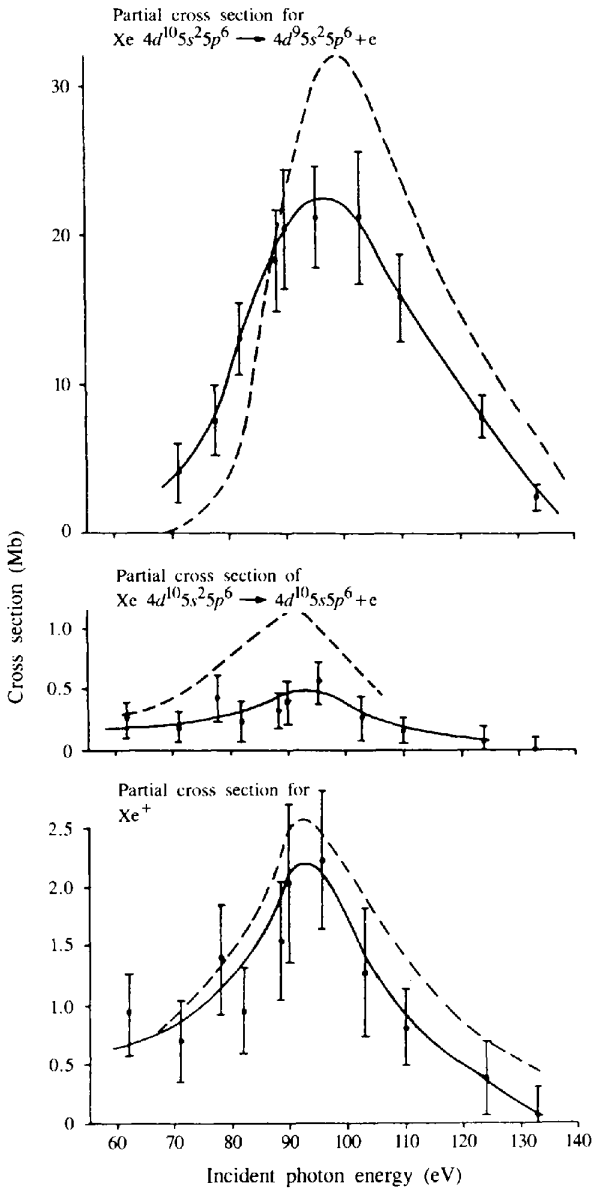

Figure 15
The partial photoionization cross sections for removal of the Xe $4d$, $5s$ and ($5s$ + $5p$) electrons (from West *et al.*, 1976).

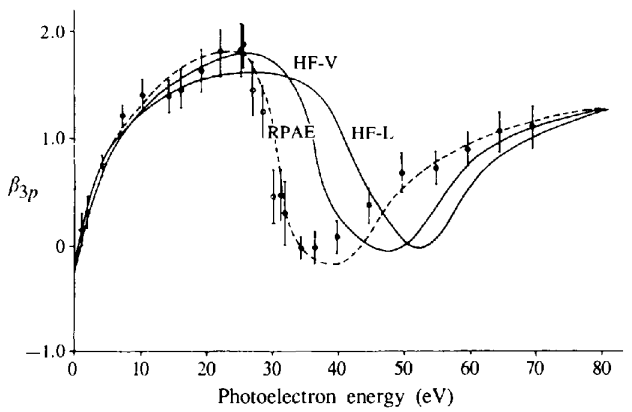

Figure 16
The variation in asymmetry parameter, β, for the Ar $3p$ electrons (from Houlgate *et al.*, 1976).

resonance, Γ. The experiment could differentiate between the $3s^23p^5\ ^2P_{1/2}$ and $^2P_{3/2}$ final states but the variation in β was found to be the same for both components. Plotted on the same figure is the $\sigma(^2P_{3/2}):\sigma(^2P_{1/2})$ branching ratio. The fact that the experimental value of 1.9:1 did not vary through the resonance region was taken as an indicator of the weakness of the spin-orbit interaction.

The variation in the total cross section, which was normalized to a value of 33 Mb at 468 Å, should have been, and indeed was, quite similar to that of Fig. 10; this simply showed that the resolution was sufficient to perform the measurement. A similar measurement on the $5s5p^66p\ ^1P_1$ resonance in Xe at 592 Å (20.95 eV) showed a variation in the $\sigma(^2P_{3/2}):\sigma(^2P_{1/2})$ ratio, indicating the effect of the increased spin-orbit splitting in Xe.

A final example, this time in the molecular context, relates to the two window resonances in O_2 seen earlier in Fig. 11. These resonances are associated with the $v = 0$ and $v = 1$ components of the neutral excited Rydberg state $(\sigma_u 2s)^{-1}\ 3s\sigma$ at 594.3 and 589.0 Å. The experiment determined the partial cross sections for leaving the O_2^+ ion in the $X\ ^2\Pi_g$ ground state as the region from 574 to 600 Å was scanned. These were further subdivided into partial cross sections for leaving the ion in a particular vibrational state of the ground electronic state. In principle, at this photon energy, one can leave the O_2^+ ion in the X, a, A, b or B states and the branching ratios in the region of the resonances could differ quite significantly from their off-resonance values (see Codling *et al.*, 1981). The net effect, however, is to produce two window resonances in the total photoabsorption cross section.

The upper curve of Fig. 18 shows the variation in the partial cross section for leaving the O_2^+ ion in its ground state, normalized to the data point of Samson, Gardner & Haddad (1977) at 584.3 Å. The surprising fact is that, whereas the total cross section shows a double minimum, the $X\ ^2\Pi_g$ state partial cross section shows a double peak! Since the total cross section shows a 6 or 7 Mb fall and the X state a 3 Mb rise, clearly one or more of the remaining partial cross sections must show quite a dramatic dip in the resonance region.

Having considered how the total cross section for leaving the O_2^+ ion in its ground state varies, one can now examine the partial cross sections for leaving the ion in a particular vibrational state; this is presented in the lower half of Fig. 18. Each component is enhanced to some extent in the resonance region, but the $v = 0$ component is particularly enhanced relative to the others. There are quite dramatic changes in the asymmetry parameter, β, on passing through the resonance region. Once again, this is particularly true of the $v = 0$ component, where the β value changes from 0.2 at 589.4 Å to −0.9 at 594.3 Å.

Before leaving the subject of photoelectron spectroscopy, it is worth mentioning the technique of threshold photo-

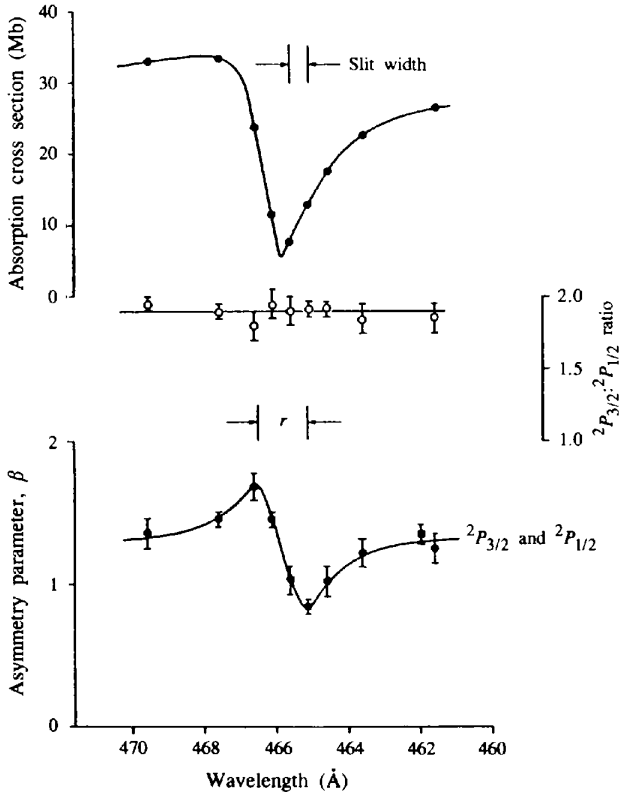

Figure 17
The photoionization cross section, the branching ratio and the asymmetry parameter, β, for the $3p$ electrons in Ar in the region of the $3s3p^6\ ^1P_1$ resonance (from Codling *et al.*, 1980).

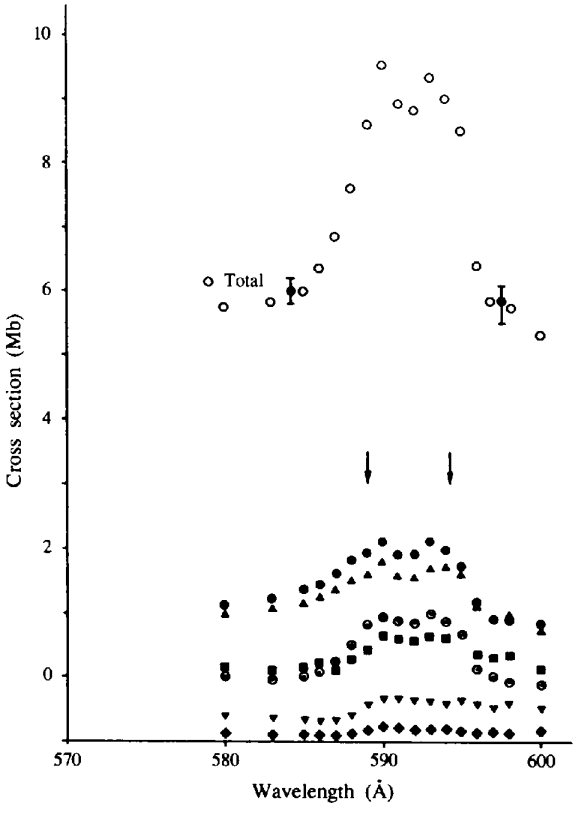

Figure 18
Partial cross section for the $X\ ^2\Pi_g$ state of O_2^+ (open circles). In the lower half the cross section is apportioned to the individual vibrational components (from Codling *et al.*, 1981).

electron spectroscopy. This technique is particularly suited to the use of a continuum source such as synchrotron radiation. If one detects threshold (*i.e.* zero-energy) electrons as a function of photon energy, one can obtain the vibrationally resolved electronic states of molecules in a rather straightforward manner. The fact that threshold electrons can be collected with high efficiency is an added advantage. As an example we show the threshold photoelectron spectrum of O_2 obtained by Guyon & Nenner (1980) in the bottom trace of Fig. 19. One sees vibrational structure associated with the *X*, *a*, *A*, *b*, *B* and *c* states mentioned earlier. In addition, one sees features in the so-called Franck–Condon gap. Here, Franck–Condon factors for direct excitation from the O_2 ground state are negligible and the structure has been interpreted in terms of an indirect mechanism, whereby the neutral molecule is excited and then autoionizes, yielding low-energy electrons.

4.2. *Mass spectrometry*

Mass spectrometry, when coupled with synchrotron radiation, can be a useful complimentary tool for studying the photoionization process. For example, the window resonances in Ar were studied using this technique (see Sorensen, Aberg, Tulkki & Kir, 1994). The top trace of Fig. 19 shows the photoionization spectrum of O_2 in the region 12–26 eV. This is the total ion spectrum (O_2^+ and O^+) and it would require separation of these ions to make full use of such an experiment.

Although photoelectron spectroscopy is recognized as the definitive technique, mass spectrometry can be of value in a situation where 'direct' double ionization occurs. This direct process leads to a continuum of electron energies that can be difficult to distinguish from a background of scattered electrons. The double ionization of Tl and Pb demonstrates this point. Although these elements are adjacent in the Periodic Table, in Tl ($5d^{10}6s^26p$) the double-ionization limit lies at an energy above the $5d$-ionization limit, whereas in Pb ($5d^{10}6s^26p^2$) it lies below. As a consequence, there is well over an order of magnitude difference in the double-ionization cross section about 5 eV above threshold. In Tl, where only direct double ionization can occur, the ratio of double-to-single ionization is 0.15; in Pb, where the Auger process can occur, it is ~5.0 (see Holland & Codling, 1980).

Schmidt *et al.* (1976) performed the first measurements on multiple ionization of the rare gases He, Ne and Ar using synchrotron radiation. Holland, Codling, West & Marr (1979) extended the measurements to Kr and Xe using ion time-of-flight (TOF) spectrometry, covering a photon energy range of 60–280 eV. It was important to keep second-order and stray light to a minimum, since it was impossible to label those ions produced by first-order radiation alone. The synchrotron was treated as a continuous source, the 'start' pulse being provided by an extraction pulse. As an example, Fig. 20 shows the absolute cross section for Ar^{2+} ions from threshold. The many-body-perturbation-theory curves of Carter & Kelly (1976) are seen to be in reasonable

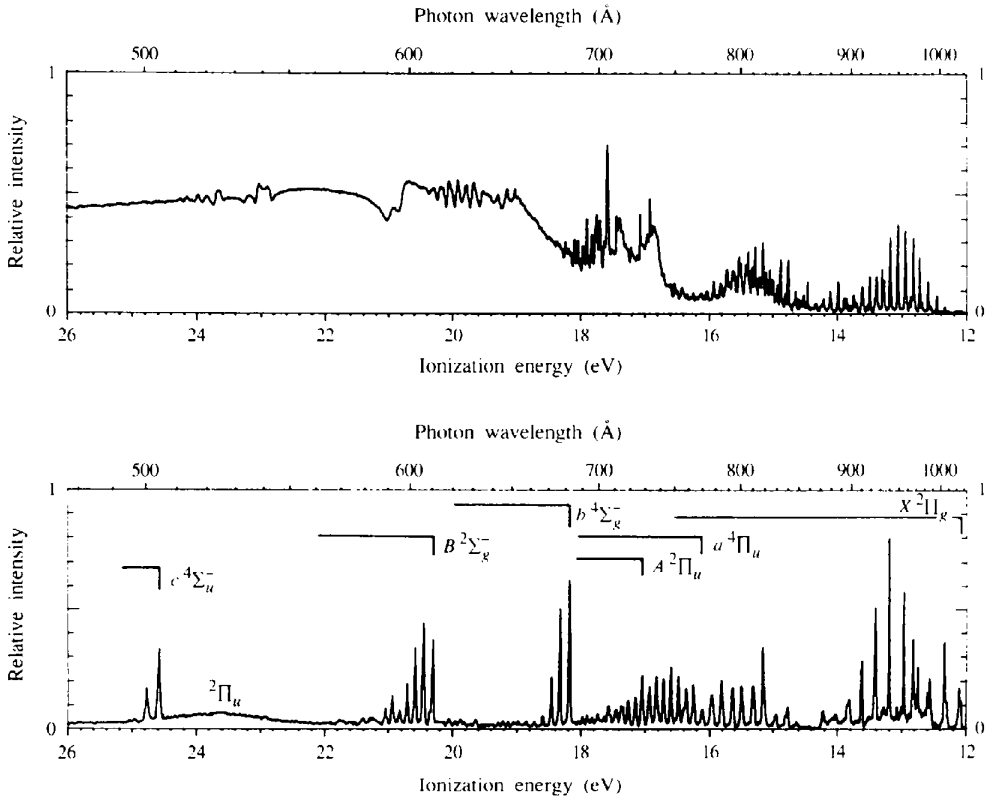

Figure 19
The total ion spectrum (top) and threshold photoelectron spectrum (bottom) of O_2 from 12–26 eV (from Guyon & Nenner, 1980).

agreement with the data. One interesting, and at the time unexplained, aspect of the curve is the steady rise in cross section prior to the L edge at 248 eV; this has recently been explained by von Busch, Ankerhold, Drees & Esser (1996).

4.3. *Fluorescence spectroscopy*

Fluorescence spectroscopy is a powerful technique when coupled with synchrotron radiation. For example, Woodruff & Samson (1982) studied the (sp, $3n$+) series in He using this technique. The $3s$ partial cross section in Ar was studied by Schartner, Mobus, Lenz, Schmoranzer & Wildberger (1988). In the case of molecules, partial photoionization cross sections can be obtained using the fluorescence excitation technique. Fig. 21, from Tabché-Fouhailé, Nenner, Guyon & Delwiche (1981), shows at the top the conventional total photoionization cross section of O_2 in the region 450–750 Å. The variation in the partial cross section for producing the $b\ ^4\Sigma_g^-$ state of O_2^+ is determined by monitoring the $b\ ^4\Sigma_g^- \rightarrow a\ ^4\Pi_u$ emission (the first negative system; see Fig. 12), whereas the $A\ ^2\Pi_u$ partial cross section is determined by monitoring the fluorescence associated with the $A\ ^2\Pi_u \rightarrow X\ ^2\Pi_g$ transition (the second negative system). One sees considerable structure in the $b\ ^4\Sigma_g^-$ cross section. Of interest in the context of the earlier discussions is that the window resonances in this cross section at ~590 Å become absorption features in the $A\ ^2\Pi_u$ partial cross section.

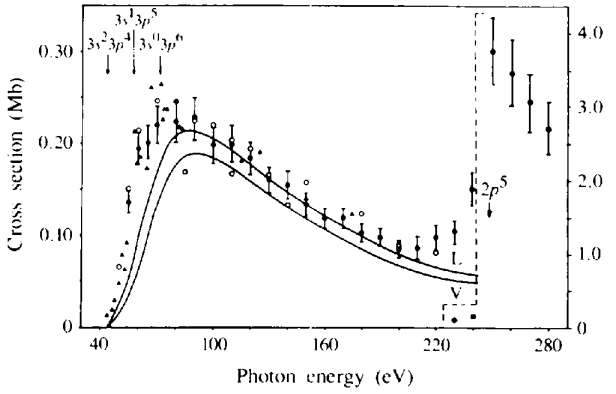

Figure 20
The Ar^{2+} absolute partial cross section (from Holland *et al.*, 1979).

4.4. *Coincidence techniques*

This is an important and expanding area which cannot be given full justice. Only three examples will be discussed; these were chosen because they involve work in which the author participated. We consider first the dissociative ionization of O_2 using the threshold photoelectron–photoion coincidence technique. Using photons in the 506–498 Å

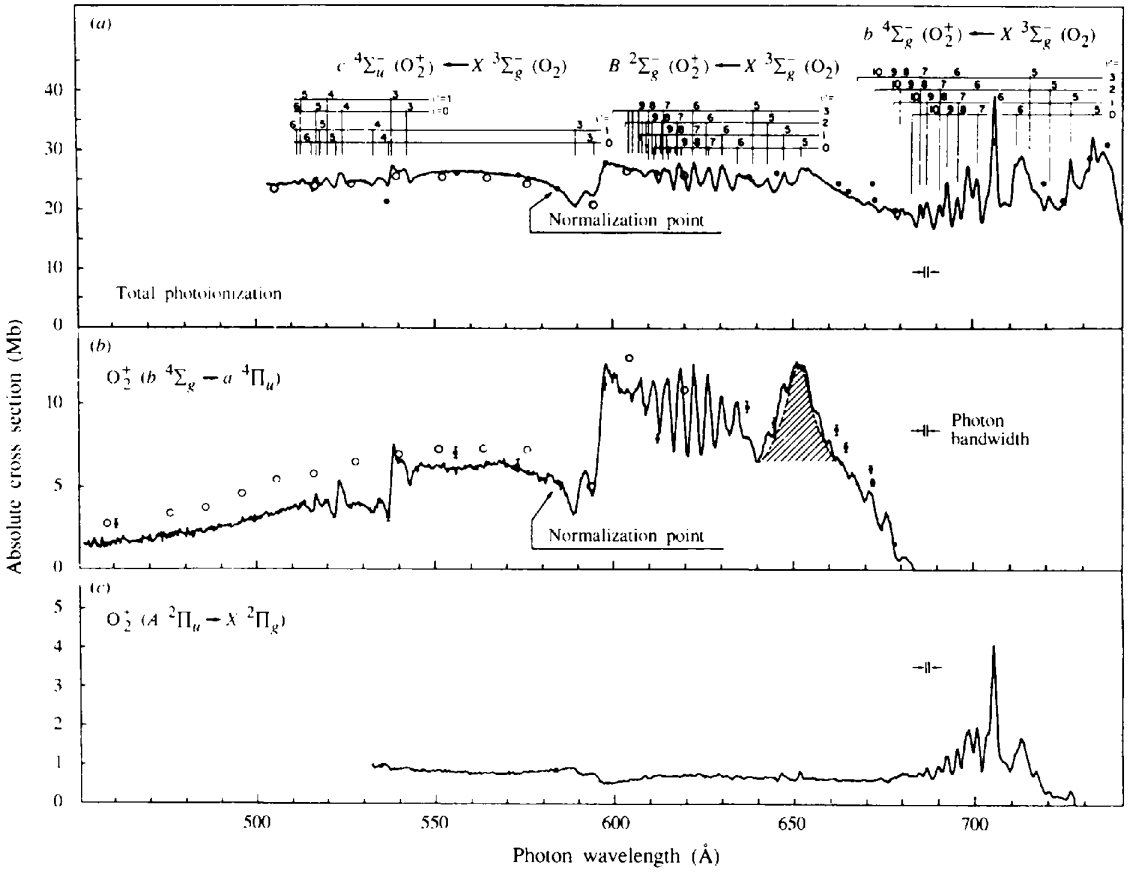

Figure 21
(*a*) The O_2^+ total photoionization cross section; (*b*) and (*c*) fluorescence spectra associated with the $b\ ^4\Sigma_g^-$ and $A\ ^2\Pi_u$ states of O_2^+ (from Tabché-Fouhailé *et al.*, 1981).

region, one observes threshold electron peaks at ~504.7 and 500.8 Å, as shown in Fig. 19. These are associated with the $v = 0$ and $v = 1$ levels of the $c\ ^4\Sigma_u^-$ state of O_2^+. Shown in Fig. 22 are the O^+-ion TOF spectra obtained in coincidence with the threshold electrons, at wavelengths λ_2 (504.7 Å) and λ_4 (500.8 Å). Three further TOF spectra are shown, taken just above 504.7 Å (λ_1), between the two (λ_3) and just below 500.8 Å (λ_5).

To follow the analysis of the O^+ TOF spectra it is useful to study Fig. 23; this shows the relevant potential energy curves and dissociation limits. Peak *A* at 15 μs results from predissociation of the $B\ ^2\Sigma_g^-$ state to a separated atom limit $O(^3P) + O^+(^4S)$ at 18.73 eV. (This, in fact, is a spurious peak; see Frasinski, Randall & Codling, 1985.) At λ_2, the $v = 0$ level of the *c* state, peak *B* involves predissociation to the limit $O(^1D) + O^+(^4S)$ at 20.70 eV and peak *C* predissociation to the limit $O(^3P) + O^+(^4S)$ at 18.73 eV. At λ_4, the $v = 1$ level of the *c* state, only one peak, *D*, is observed. This suggests that predissociation occurs predominantly, if not entirely, to the limit $O(^1D) + O^-(^4S)$ at 20.70 eV. Because of the shallowness of the *c*-state potential well, it is probable that tunnelling contributes to the observation of peak *D* at λ_4 ($v = 1$), but at λ_2 ($v = 0$) conventional predissociation must predominate.

We consider now a triple coincidence experiment, a photon–photoelectron–photoion experiment. This coincidence technique utilized the 'single-bunch' mode of operation of the Daresbury SRS, when the radiation is emitted in 0.2 ps pulses at intervals of 2 ps. No field was applied across the interaction region and the electrons and ions moved with energies dictated solely by the photoionization process. The electrons and ions were detected using two coaxial drift tubes. A photoelectron provided the 'start' pulse, the light pulse (the monochromatic radiation) and the photoion the two 'stop' pulses. Here, the axes of a three-dimensional map are electron TOF (*x* axis), ion TOF (*y* axis) and coincidence counts (*z* axis).

Such a triple coincidence technique has been used to probe the predissociation of O_2 at 486 Å (25.5 eV) (see Frasinski, Stankiewicz, Randall, Hatherly & Codling, 1986). Fig. 23 indicates that this is less than 1 eV above the $v = 1$ level of the $c\ ^4\Sigma_u^-$ state of O_2^+. A false-colour map produced at this wavelength is shown in Fig. 24(*a*). The continuous horizontal and vertical lines are due to cross talk and false coincidences and are of no interest, except that they confirm the electron TOF (energy) scale. The features labelled *B* and *c* in the accompanying Fig. 24(*b*) can be understood in terms of the potential energy curves in Fig. 23. Feature *B* is associated with electrons of 5.3 eV energy and ions of 0.9 eV energy. The O^+ ions are clearly produced in the predissociation of the $B\ ^2\Sigma_g^-$ state to the limit $O(^3P) + O^+(^4S)$, as discussed earlier. The lowest feature on the diagram is associated with predissociation of the $v = 0$ level of the *c* state to the same limit, with an O^+ energy of ~3 eV. The feature directly above is associated with predissociation of the same $v = 0$ level to the limit $O(^1D) + O^-(^4S)$, with an O^+ energy of ~2 eV.

There is only one feature associated with the $v = 1$ level because tunnelling to the final products $O(^1D) + O^+(^4S)$ is much faster than any possible predissociation process to the limit $O(^3P) + O^-(^4S)$. We see, then, that such a triple coincidence map gives a very visual corroboration of the earlier interpretation of Frasinski *et al.* (1985). Indeed, this visual display allows an immediate insight into the various correlated events at a single wavelength. The continuous features labelled 1 and 2 can be assigned to repulsive states.

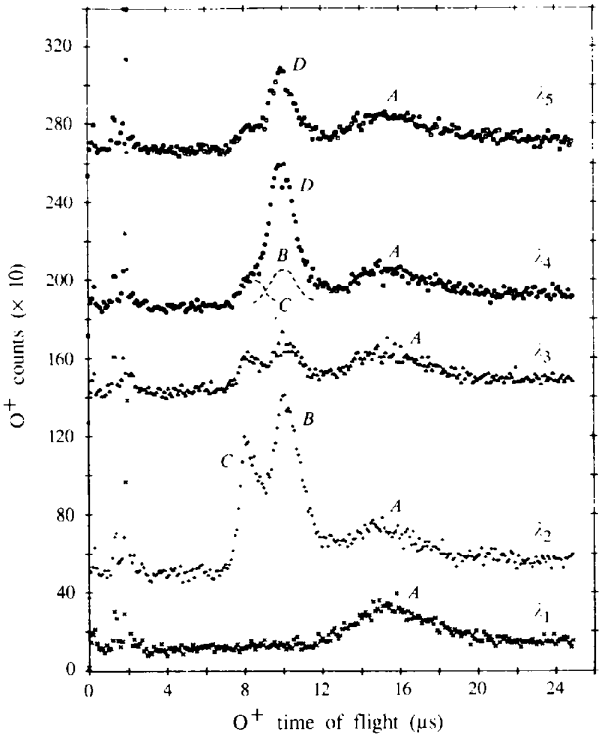

Figure 22
O^+-ion TOF spectra at wavelengths λ_1–λ_5 indicated on Fig. 23. The labelling of the peaks is discussed in the text (from Frasinski *et al.*, 1985).

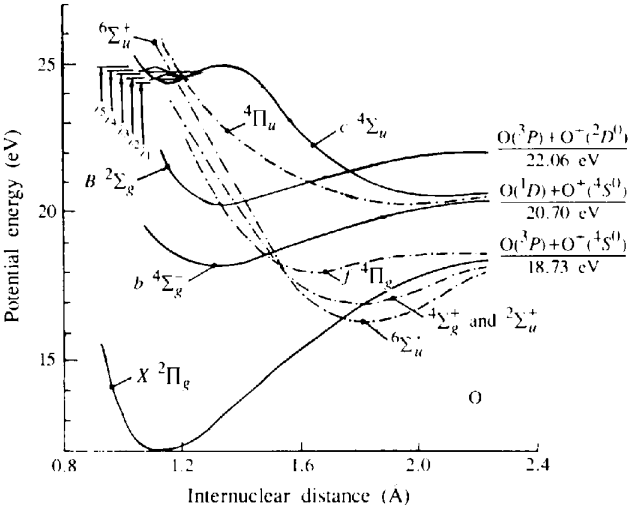

Figure 23
Potential energy curves for O_2^+; see Fig. 22.

Feature 2 had already been recognized as a broad peak in the conventional threshold photoelectron spectroscopy spectrum of O_2 centred at 23.6 eV and labelled $^2\Pi_u$ in Fig. 19. However, in the region 22–24 eV there are signs of a second repulsive state (labelled 1), which leads to the dissociation limit $O(^3P) + O^+(^4S)$. This could not be recognized in a conventional electron TOF spectrum since such a spectrum would be the result of projecting all features on the map onto the x axis and the weaker feature would be overwhelmed by the stronger one.

A second example of triple coincidence is the photoelectron–photoion–photoion coincidence experiment. When it was introduced by Frasinski *et al.* (1986) the photoion–photoion coincidence was already in use (see, for example, Dujardin, Leach, Dutuit, Guyon & Richard-Vierd, 1984). In the photoion–photoion coincidence approach, two ions are detected using a single drift tube plus detector and the time difference, Δt, between their TOF's is determined. If Δt_{max} and Δt_{min} are the maximum and minimum time difference for a particular pair of ions produced in a dissociation process, then $(\Delta t_{max} + \Delta t_{min})/2$ determines the ionic fragments and $(\Delta t_{max} - \Delta t_{min})/2$ determines the kinetic energy of the fragments.

There is a potential problem using the photoion–photoion coincidence approach, in that ions may arrive with the same time difference but from different ion pairs with different kinetic energy releases. This problem is overcome in the photoelectron–photoion–photoion coincidence approach. Here, the *absolute* TOF of each fragment is determined. Two drift tubes are required, one for electrons, one for ions, and these are placed coaxially either side of the photon–molecule interaction region. At a specific incident photon energy the various fragmentation channels are displayed in the form of a three-dimensional map. The x axis is labelled TOF of ion 1, the y axis is labelled TOF of ion 2 and the z axis is coincidence counts. The map contains islands or features in the form of a dumb-bell, with its axis lying at an angle determined by the ratio of the ion charges. The length gives the dissociation energy and the total number of counts in the feature gives the partial cross section for producing a particular ion pair (if collection and detection efficiencies are known). For example, Stankiewicz, Hatherly, Frasinski, Codling & Holland (1989) have studied NH_3 in the region of the double-ionization threshold. One observes the following channels (and threshold energies): $NH_2^+ + H^+$ (35.7 eV); $NH^+ + H^+$ (43.3 eV); $N^+ + H^+$ (49.2 eV). The problem of false coincidences in such an approach has been, to a large extent, solved by Frasinski, Stankiewicz, Hatherly & Codling (1992).

There are many more coincidence experiments being actively pursued at the present time, too numerous to mention here. For example, experiments are able to measure the angular distribution and energies of both the electrons and ions emitted in the double-ionization process, in coincidence. It is clear that many of these techniques will find their greatest application with third-generation synchrotron radiation sources.

I would like to take this opportunity to thank my many friends at the NBS (now NIST), Daresbury, Reading and elsewhere for helping to make much of the work described here so rewarding. I would like to dedicate this contribution to Dr Karl G. Kessler, Chief of the Atomic Physics Division during my stay at the NBS; his enthusiasm and encouragement were very much appreciated.

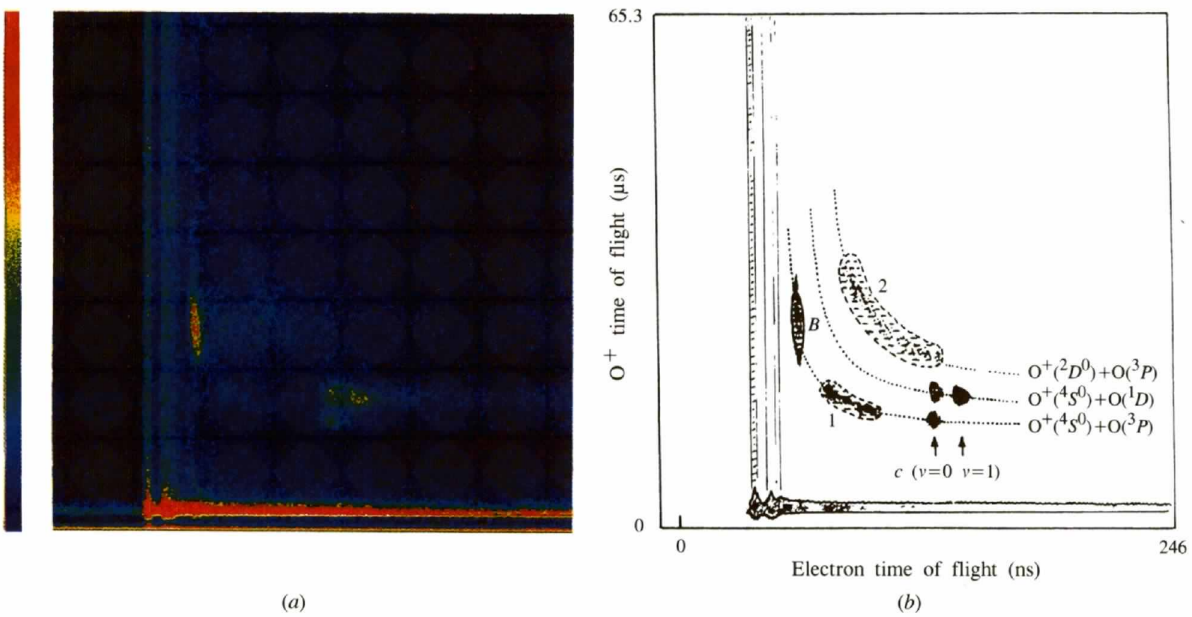

Figure 24
(*a*) Electron–ion coincidence map, showing predissociation mechanisms in O_2^+ at a wavelength of 486 Å (25.5 eV). (*b*) The various features in (*a*) are sketched here, labelled, and discussed in the text (from Frasinski *et al.*, 1986).

References

Amusia, M. Ya., Ivanov, V. K., Cherepkov, N. A. & Chernysheva, L. V. (1972). *Phys. Lett. A*, **40**, 361.

Amusia, M. Ya., Ivanov, V. K., Cherepkov, N. A. & Chernysheva, L. V. (1974). *Sov. Phys. JETP*, **39**, 752–758.

Asbrink, L., Fridh, C., Lindholm, E. & Codling, K. (1974). *Phys. Scr.* **10**, 183–185.

Balzer, P., Lundqvist, M., Wannberg, B., Karlsson, L., Larsson, M., Hayes, M. A., West, J. B., Siggel, M. R. F., Parr, A. C. & Dehmer, J. L. (1994). *J. Phys. B*, **27**, 4915–4932.

Beutler, H. (1935). *Z. Phys.* **93**, 177–196.

Burke, P. G., McVicar, D. D. & Smith, K. (1963). *Phys. Rev. Lett.* **11**, 559–561.

Burke, P. G. & Taylor, K. T. (1975). *J. Phys. B*, **8**, 2620–2639.

Busch, F. von, Ankerhold, U., Drees, S. & Esser, B. (1996). *J. Phys. B*, **29**, 5343–5350.

Carter, S. L. & Kelly, H. P. (1976). *J. Phys. B*, **9**, L565–568.

Codling, K. (1966*a*). *Astrophys. J.* **143**, 552–558.

Codling, K. (1966*b*) *J. Chem. Phys.* **44**, 4401–4402.

Codling, K. & Madden, R. P. (1963). *Phys. Rev. Lett.* **10**, 516–518.

Codling, K. & Madden, R. P. (1964). *Phys. Rev. Lett.* **12**, 106–108.

Codling, K. & Madden, R. P. (1965*a*). *J. Appl. Phys.* **36**, 380–387.

Codling, K. & Madden, R. P. (1965*b*). *Appl. Opt.* **4**, 1431–1434.

Codling, K. & Madden, R. P. (1965*c*). *J. Chem. Phys.* **42**, 3935–3938.

Codling, K. & Madden, R. P. (1968). *Phys. Rev.* **167**, 587–591.

Codling, K. & Madden, R. P. (1972). *J. Res. Natl Bur. Stand. Sect. A*, **76**, 1–12.

Codling, K., Madden, R. P. & Ederer, D. L. (1967). *Phys. Rev.* **155**, 26–37.

Codling, K. & Mitchell, P. (1970). *J. Phys. E*, **3**, 685–689.

Codling, K., Parr, A. C., Ederer, D. L., Stockbauer, R. L., West, J. B., Cole, B. E. & Dehmer, J. L. (1981). *J. Phys. B*, **14**, 657–666.

Codling, K. & Potts, A. N. (1974). *J. Phys. B*, **7**, 163–169.

Codling, K., West, J. B., Parr, A. C., Dehmer, J. L. & Stockbauer, R. L. (1980). *J. Phys B*, **13**, L693–697.

Cooper, J. W. (1962). *Phys. Rev.* **128**, 681.

Cooper, J. W., Conneely, M. J., Smith, K. & Ormonde, S. (1970). *Phys. Rev. Lett.* **25**, 1540–1543.

Cooper, J. W., Fano, U. & Prats, F. (1963). *Phys. Rev. Lett.* **10**, 518–521.

Cooper, J. W. & Zare, R. N. (1968). *J. Chem. Phys.* **48**, 942–943.

Dibeler, V. H. & Mohler, F. L. (1948). *J. Res. Natl Bur. Stand.* **40**, 25.

Domke, M., Remmers, G. & Kaindl, G. (1992). *Phys. Rev. Lett.* **69**, 1171–1174.

Dujardin, G., Leach, S., Dutuit, O., Guyon, P. M. & Richard-Vierd, M. (1984). *Chem. Phys.* **88**, 339–353.

Ederer, D. L. (1964). *Phys. Rev. Lett.* **13**, 760–762.

Ederer, D. L., Lucatorto, T. & Madden, R. P. (1970). *Phys. Rev. Lett.* **25**, 1537–1540.

Elder, F. R., Gurewitsch, M., Langmuir, R. V. & Pollock, H. C. (1947). *Phys. Rev.* **71**, 829–830.

Fano, U. (1935). *Nuovo Cimento*, **12**, 156–161.

Fano, U. (1961). *Phys. Rev.* **124**, 1866–1878.

Fano, U. & Cooper, J. W. (1965). *Phys. Rev. A*, **137**, 1364–1379.

Frasinski, L. J., Randall, K. J. & Codling, K. (1985). *J. Phys. B*, **18**, L129–135.

Frasinski, L. J., Stankiewicz, M., Hatherly, P. A. & Codling, K. (1992). *Meas. Sci. Technol.* **3**, 1181–1191.

Frasinski, L. J., Stankiewicz, M., Randall, K. J., Hatherly, P. A. & Codling, K. (1986). *J. Phys. B*, **19**, L819–824.

Garton, W. R. S. (1959). *J. Sci. Instrum.* **36**, 11–16.

Garton, W. R. S. & Codling, K. (1965). *Proc. Phys. Soc.* **86**, 1067–1075.

Gilmore, F. R. (1965). *J. Quant. Spectrosc. Radiat. Transfer*, **5**, 369–389.

Gudat, W. & Kunz, C. (1979). In *Synchrotron Radiation: Techniques and Applications*, edited by C. Kunz. Berlin: Springer-Verlag.

Guyon, P. M. & Nenner, I. (1980). *Appl. Opt.* **19**, 4068–4079.

Holland, D. M. P. & Codling, K. (1980). *J. Phys. B*, **13**, L745–748.

Holland, D. M. P., Codling, K., West, J. B. & Marr, G. V. (1979). *J. Phys. B*, **12**, 2465–2484.

Hopfield, J. J. (1930*a*). *Phys. Rev.* **35**, 1133.

Hopfield, J. J. (1930*b*). *Phys. Rev.* **36**, 789.

Houlgate, R. G., West, J. B., Codling, K. & Marr, G. V. (1976). *J. Electron Spectrosc. Relat. Phenom.* **9**, 205–209.

Joos, P. (1960). *Phys. Rev. Lett.* **4**, 558.

Kelly, H. P. & Simons, R. L. (1973). *Phys. Rev. Lett.* **30**, 529.

Kennedy, D. J. & Manson, S. T. (1972). *Phys. Rev. A*, **5**, 227.

Leblanc, F. J. (1963). *J. Chem. Phys.* **38**, 487–488.

Lyman, T. (1926). *Science*, **64**, 89–90.

Lynch, M. J., Gardner, A. B., Codling, K. & Marr, G. V. (1973). *Phys. Lett. A*, **43**, 237–238.

Madden, R. P. & Codling, K. (1963). *Phys. Rev. Lett.* **10**, 516–518.

Madden, R. P. & Codling, K. (1965). *Astrophys. J.* **141**, 364–375.

Madden, R. P., Ederer, D. L. & Codling, K. (1967). *Appl. Opt.* **6**, 31–38.

Madden, R. P., Ederer, D. L. & Codling, K. (1969). *Phys. Rev.* **177**, 136–151.

Mitchell, P. & Codling, K. (1972). *Phys. Lett. A*, **38**, 31–32.

Narayama, B. & Price, W. C. (1972). *J. Phys. B*, **5**, 1784–1789.

Nordfors, B. (1955). *Arkiv. Fys.* **10**, 20.

Samson, J. A. R., Gardner, J. L. & Haddad, G. N. (1977). *J. Electron Spectrosc. Relat. Phenom.* **12**, 281–292.

Schartner, K. H., Mobus, B., Lenz, P., Schmoranzer, H. & Wildberger, M. (1988). *Phys. Rev. Lett.* **61**, 2744–2747.

Schmidt, V., Sandner, N., Kuntzemuller, H., Dhez, P., Wuilleumier, F. & Kallne, E. (1976). *Phys. Rev. A*, **13**, 1748.

Schwinger, J. (1949). *Phys. Rev.* **75**, 1912–1925.

Silverman, S. M. & Lassettre, E. N. (1964). *J. Chem. Phys.* **40**, 1265–1271.

Sorensen, S. L., Aberg, T., Tulkki, J. & Kirm, M. (1994). *Phys. Rev. A*, **50**, 1218–1230.

Stankiewicz, M., Hatherly, P. A., Frasinski, L. J., Codling, K. & Holland, D. M. P. (1989). *J. Phys. B*, **22**, 21–31.

Tabché-Fouhailé, A., Nenner, I., Guyon, P. M. & Delwiche, J. (1981). *J. Chem. Phys.* **75**, 1129–1138.

Tanaka, Y. & Takamine, T. (1942). *Sci. Pap. Inst. Phys. Chem. Res. (Jpn)*, **39**, 437.

Tomboulian, D. H. & Hartman, P. L. (1956). *Phys. Rev.* **102**, 1423–1447.

Vidal, C. R. & Cooper, J. (1969). *J. Appl. Phys.* **40**, 3370–3374.

Weissler, G. L. (1971). *Sci. Light*, **20**, 95–99.

West, J. B., Woodruff, P. R., Codling, K. & Houlgate, R. G. (1976). *J. Phys. B*, **9**, 407–410.

Whiddington, R. & Priestley, H. (1934). *Proc. R. Soc. London Ser. A*, **145**, 462.

Woodruff, P. R. & Samson, J. A. R. (1982). *Phys. Rev. A*, **25**, 848–856.